Mon. Not. R. astr. Soc. (1985) **216,** 467–502

Triaxial galaxies containing massive black holes or central density cusps

Ortwin E. Gerhard *Max-Planck-Institut für Astrophysik, D-8046 Garching b. München, F.R. Germany*

James Binney *Department of Theoretical Physics, Keble Road, Oxford OX1 3NP*

Accepted 1985 April 30. Received 1985 April 30; in original form 1985 March 8

Summary. The box orbits that form the backbone of a triaxial elliptical galaxy carry stars arbitrarily close to the centre. In this paper we investigate how these orbits are affected if either (i) a massive black hole lurks at the centre, or (ii) the stellar density becomes arbitrarily large near the centre.

Elementary considerations show that a point mass at the centre will eventually disrupt the crucial box orbits by subjecting stars on these orbits to large-angle deflections. Numerical experiments show that the time-scale for disruption of box orbits by weaker encounters is comparable with the time for disruption by these hard encounters, and that the disruptive effect of the central mass can be modelled by a series of discrete scattering events.

We argue that over a Hubble time a central black hole with 2 per cent of the core mass will disrupt most box orbits with apocentres interior to about 1 kpc. This may lead to an abrupt loss of triaxiality throughout the galaxy, but a simple calculation suggests that the loss of triaxiality will be confined to the centre.

We calculate that a $10^8 M_\odot$ black hole at the centre of a typical giant elliptical is currently disrupting stars at a rate $\simeq 4\times10^{-6} M_\odot\,\mathrm{yr}^{-1}$ if the galaxy is triaxial, and $\simeq 2\times10^{-7} M_\odot\,\mathrm{yr}^{-1}$ if it is axisymmetric.

We show that regular box orbits persist in systems with singular central densities such as that implied by carrying the $r^{1/4}$ law all the way to $r=0$. Indeed, at low energies, Schwarzschild's model allows fewer box orbits than a model with the same axis ratios in which the central density diverges at the centre as in the standard $r^{1/4}$ model.

1 Introduction

In recent years it has been widely argued that elliptical galaxies are triaxial bodies (e.g. Binney 1982a and references therein). Observational evidence (Evans 1952; King 1978; Illingworth 1977; Binney 1985) that many elliptical galaxies cannot be rotationally flattened oblate axisymmetric bodies, has been strongly supported by *n*-body simulations (Aarseth & Binney 1978; Hohl &

Zang 1979; Wilkinson & James 1981; Gerhard 1983) and orbit integrations in fixed gravitational potentials (Schwarzschild 1979, 1982) which have demonstrated that self-consistent triaxial stellar systems are dynamically possible. However, existing theoretical models cannot represent real elliptical galaxies in one important respect; the models have homogeneous cores in which the gravitational potential is an approximately quadratic function of the coordinates, while giant ellipticals often have central cusps of brightness (Schweizer 1979; Lauer 1985), and may additionally contain massive black holes in their nuclei (Lynden-Bell 1969; Sargent *et al.* 1978; Rees 1984). Simple arguments suggest that such feature may be incompatible with existing theories of triaxial stellar systems (Norman & Silk 1983).

In Section 2 we summarize our understanding of the dynamics of triaxial elliptical systems and indicate why the failure of existing triaxial galaxy models to include a central density cusp or compact object may have important dynamical consequences. In Sections 3 and 4 we examine the consequences of placing a massive black hole at the centre of a triaxial galaxy. This problem has recently been treated by Norman, May & van Albada (1985), and some features of our discussion parallel theirs. However, we concentrate on analysis of orbits in given potentials, rather than discussing n-body models, since Norman, May & van Albada show that unwanted discreteness effects drive spurious relaxation in current n-body models. In Section 3 we study the breakdown of the all-important box orbits under the influence of a central massive body, through a series of surfaces of section, and construct a simple scattering model of our results that enables us to predict the time required to disrupt most box orbits of any given scale. In Section 4 we discuss the effect this disruption will have on the shape of an initially triaxial system, and estimate the rate at which a black hole at the centre of a triaxial galaxy can tidally shred stars.

In Section 5 we compare orbits in models having homogeneous cores with orbits in models in which the density diverges at small radii, and conclude that triaxial systems can have singular central densities of the type predicted by carrying de Vaucouleurs' $r^{1/4}$ law right into the centre, but that a central cusp so pronounced that the circular speed diverges as the centre is approached eliminates the box orbits.

2 Stellar orbits and triaxiality

If elliptical galaxies are triaxial, the smoothness of their brightness profiles out to several effective radii strongly suggests that the major rotation-related resonances, for example the inner Lindblad and corotation resonances, lie well outside the main bodies of these galaxies. Hence the figures of elliptical galaxies can rotate slowly, if at all, and the main features of triaxial elliptical galaxies are probably accurately represented by models whose figures do not rotate.

Schwarzschild (1979) constructed a self-consistent triaxial model in a non-rotating potential. Most orbits in his system are of three types: box orbits, long-axis tubes and short-axis tubes. All these orbits respect three effective isolating integrals. We call such orbits *regular*. Orbits respecting fewer than three effective isolating integrals we call *irregular*. The most heavily populated orbits in Schwarzschild's model are the elongated box orbits. Indeed it is these orbits which provide the backbone of the system in the sense that it is these orbits which keep the overall density high along the longest and intermediate axes by comparison with the shortest axis. By contrast, the fat box orbits and orbits of the two tube families always enhance the density more parallel to one of the shorter two axes than they do parallel to the longer two axes. Thus it seems likely that a triaxial galaxy can be constructed around a non-rotating triaxial potential only if the potential admits a range of elongated box orbits that can be selectively populated to form the backbone of the galaxy.

Stars on box orbits repeatedly pass close to the centre, and eventually reach arbitrarily small radii. At points near the centre of the potential, the elongated box orbits of the galaxy's backbone

differ from fat box orbits of the same energy by the directions of their velocity vectors. A feature in the galaxy's potential that can scatter stars will shift them from one box orbit to another and thus tend to populate all box orbits equally. The consequent depopulation of the elongated box orbits must then dissolve the galaxy's backbone. Candidate features include the potentials of black holes and central density cusps.

3 Effect of central compact object on box orbits

It is likely that black holes or other compact objects which once powered radio galaxies and quasars, lurk at the centres of many giant elliptical galaxies. A variety of arguments suggest that these objects have masses of the order of $10^8 M_\odot$ (Begelman, Blandford & Rees 1984). By comparison the formal 'core mass' (Kormendy 1982) of a typical giant elliptical is of order $5\times10^9 M_\odot$. Hence in this section we ask how orbits in a triaxial elliptical galaxy are affected by the introduction at the centre of a compact object containing of order 2 per cent of the total mass of the galaxy core.

3.1 ANALYTIC ESTIMATES

For simplicity we assume that the underlying galaxy potential Φ_G has a harmonic core, and we neglect the gravitational attraction of the cusp of stars that is expected to accumulate around the central compact object; from the work of Young (1978, 1980) one may verify that for parameters of interest, the mass of such a cusp is much smaller than the mass of the central object. With these approximations, the gravitational force generated by the core material rises linearly with radius r;

$$F_G \simeq \frac{v_c^2}{r_c^2} r \qquad (r<r_c) \tag{1}$$

where v_c is the circular speed at the edge $r=r_c$ of the core. The gravitational force F_h generated by the central compact object of mass m varies as r^{-2}.

$$F_h = \frac{Gm}{r^2}. \tag{2}$$

Hence the attraction of the compact object dominates the force field interior to*

$$r_h = \mu^{1/3} r_c \tag{3}$$

where

$$\mu \equiv \frac{Gm}{r_c v_c^2} = \frac{m}{M_c}. \tag{4}$$

Here

$$M_c \equiv \frac{r_c v_c^2}{G} \tag{5}$$

is the core mass. We are interested in the response of orbits to the introduction of central masses such that $\mu \simeq 0.02$.

*Note that r_h as defined here is larger than the quantity R_h defined by Frank & Rees (1976) and by Norman, May & van Albada (1985) by a factor of order $(r_c/r_h)^2$.

A star on a box orbit in a non-rotating potential eventually passes arbitrarily close to the centre of the galaxy. Hence at some time it will enter the region $r<r_h$ in which the central object dominates the force-field. Inside $r=r_h$ the orbit is effectively Keplerian. Let v_h be the star's speed at r_h. Then v_h^2 is made up of a contribution from the basic galaxy potential Φ_G, and a contribution from the potential of m. Since at $r>r_h$, Φ_G provides the greater force,

$$v_h \simeq \sqrt{[2\{\Phi_G(a)-\Phi_G(r_h)\}]} \tag{6}$$

where a is the maximum distance to which a star of the given energy can go down the galaxy's long axis. There are two cases to consider:

(i) $a \simeq r_h$: In this case $(1/2)v_h^2 < Gm/r_h$ and the Kepler orbit is bound. Essentially all orbits in this regime are loop orbits rather than the nearly simple-harmonic box orbits that in the absence of the central object dominate motion in the core of the galaxy.

(ii) $a \gg r_h$: Now $(1/2)v_h^2 > Gm/r_h$ and the orbit is hyperbolic. Inside r_h it may be approximated by a pure Keplerian orbit with asymptotic speed v_h. The star's deflection along the orbit is large if the orbit is near parabolic, that is, if the effective impact parameter b of the encounter is less than the value

$$b_l = \frac{Gm}{v_h^2} = \mu\left(\frac{v_c}{v_h}\right)^2 r_c \tag{7}$$

associated with deflection through 90°. On each crossing of the galaxy core, the star has to pass through the narrow waist of its box orbit. Let the area of this waist be A, and assume that the orbit passes through each part of A with equal probability. (Numerical integrations presented below approximately verify the analogous assumption for planar orbits.) We then expect the star to be scattered through a large angle after $A/\pi b_l^2$ passages through the centre. As Fig. 1 indicates, this scattering may be thought of as moving the star to a new box orbit, from which a second scattering will move it to a third box orbit, and so on. These scattering events will tend to undermine the triaxiality of the galaxy by distributing stars uniformly amongst the box orbits. Note also that repeated shifts from one quasi-periodic motion to another are characteristic of irregular orbits. Hence we expect even a small central mass to destroy the regularity of all box orbits.

The following simple example will illustrate these ideas. Let Φ_G be the logarithmic potential

$$\Phi_L = \frac{1}{2}v_L^2 \ln\left(x^2 + \frac{y^2+z^2}{q^2} + r_c^2\right), \tag{8}$$

where v_L^2 is the characteristic speed of large loop orbits. Since at $x=r_c$ we have $v_c^2=\frac{1}{2}v_L^2$, equations (6) and (7) yield

$$b_l = \frac{\mu r_c}{2\ln\{(a^2+r_c^2)/(r_h^2+r^2{}_c)\}}. \tag{9}$$

When $\mu=0.02$, $a=0.9r_c$, we obtain $b_l=0.96\mu r_c$, and when $\mu=0.02$, $a=7r_c$ we find $b_l=0.13\mu r_c$.

A typical giant elliptical galaxy might have a central velocity dispersion $\sigma_c=240\,\mathrm{km\,s^{-1}}$. For an isothermal core, this corresponds to $v_c\simeq 300\,\mathrm{km\,s^{-1}}$, and using Kormendy's (1982) correlation of core properties, $r_c\simeq 240\,\mathrm{pc}$, and $M_c\simeq 5\times10^9\,M_\odot$. The time between passages through the nucleus is the dynamical time

$$\tau_{dyn} \simeq \frac{2a}{v_c} \simeq 1.6\times10^6 \frac{a}{r_c}\,\mathrm{yr}. \tag{10}$$

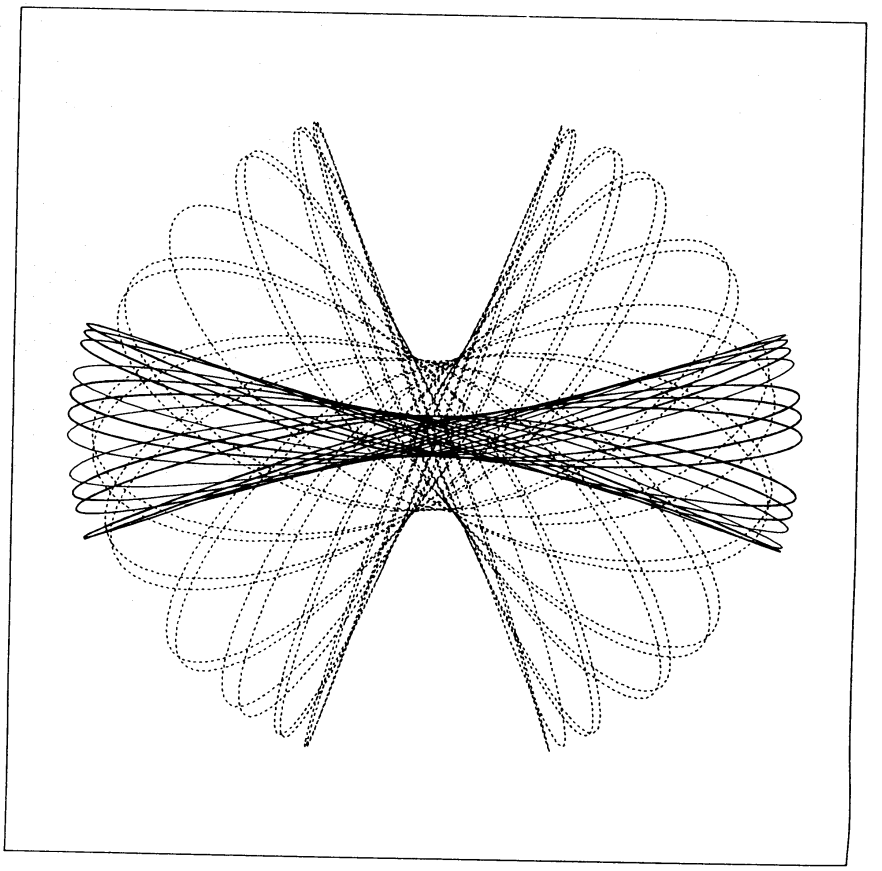

Figure 1. Two planar box orbits of the same energy (corresponding to $a=7r_c$) in the logarithmic potential (8). The effect of scattering by a central object is to move the star from one such orbit to another.

Typical box orbits have waists that are about $2r_c$ on a side. Hence the time τ_l between hard encounters with the central object is

$$\tau_l \equiv \frac{(2r_c)^2}{\pi b_l^2}\tau_{dyn} \simeq 2.0\times10^6\left(\frac{r_c a}{b_l^2}\right)\text{yr}. \tag{11}$$

Thus $\tau_l(a=0.9r_c)\simeq 2.0\times10^6/\mu^2$ yr and $\tau_l(a=7r_c)\simeq 8.3\times10^8/\mu^2$ yr. Notice that since $b_l\propto\mu$, $\tau_l\propto\mu^{-2}$ and there is a critical mass $\mu_{dis}(a)$ that is capable of destroying by hard encounters most box orbits of scale a by the present epoch. Numerically $\mu_{dis}(0.9r_c)\simeq 0.014$ and $\mu_{dis}(7r_c)\simeq 0.29$.

Thus although hard encounters with a central object are in principle capable of scattering stars from an box orbit, stars on orbits that extend well out of the core of the galaxy are unlikely to have suffered a large-angle deflection by the present epoch unless the central mass is rather larger ($m\geq 10^9 M_\odot$) than one might have anticipated from studies of quasars and radio galaxies.

3.2 NUMERICAL INTEGRATIONS

3.2.1 Surfaces of section

The arguments just presented provide upper limits to the time during which box orbits may appear regular in the presence of a central compact object, but they cannot demonstrate that box orbits remain regular in the face of repeated weak encounters with a central black hole. Therefore we now present the results of numerical integrations of box orbits in the logarithmic potential (8) with $q=0.9$.

Some care is called for when integrating these orbits since stars on such orbits are subject to large accelerations when they pass close to the central object. We have employed a fourth-order Runge–Kutta algorithm with time-step length Δt determined as described in the Appendix. As discussed in the Appendix, we have tested the reliability of this algorithm by integrating highly eccentric orbits in a Kepler potential and comparing the numerical and analytic solutions.

Schwarzschild (1979) and de Zeeuw (1985a) have shown that general box orbits may be thought of as developments of those box orbits which are confined to the plane of the system containing the longest and intermediate axes of the potential. [Following Schwarzschild (1979) we refer to this as the plane $z=0$.] If these planar box orbits are irregular, more general box orbits are unlikely to be regular. Hence in this paper we concentrate on the structure of orbits in the plane $z=0$.

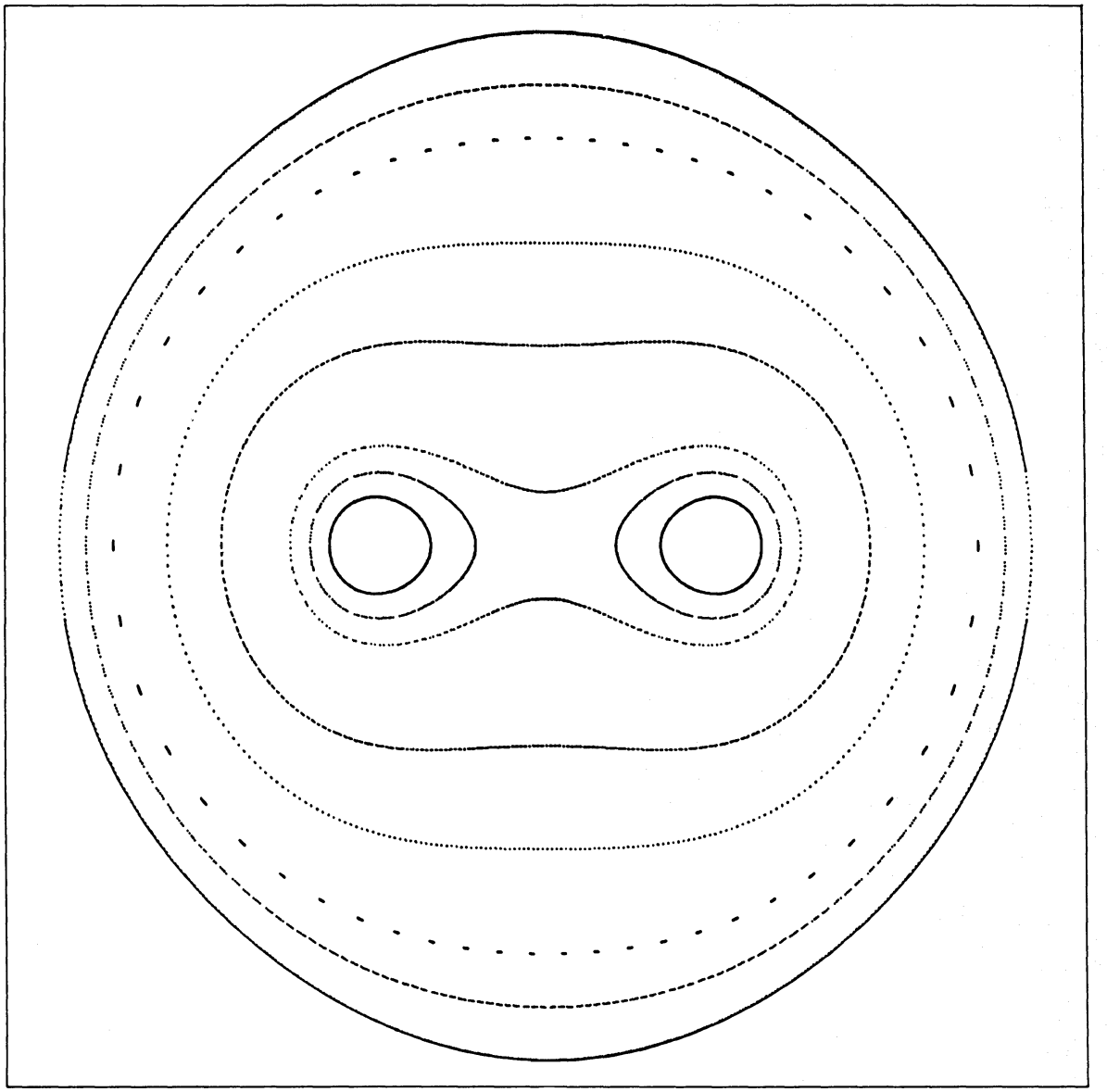

(a)

Figure 2. $(x, \dot{x})$ surfaces of section for motion in the potential of a central Plummer model, mass $m=\mu M_c$, scale-length ε added to the potential Φ_L defined by equation (8). All three surfaces of section are at energy corresponding to $a=0.9r_c$. The parameters of the central body are: (a) $\mu=0$; (b) $\mu=0.02, \varepsilon=0.07r_c$; (c) $\mu\simeq0.02, \varepsilon\simeq0.05r_c$. For clarity, in this and all subsequent surfaces of section, the ordinate is not $\dot{x}$ but $\ln(1+\frac{1}{4}\dot{x})$.

We take the central object to be a Plummer model with potential

$$\Phi_h = \frac{-Gm}{\sqrt{(r^2+\varepsilon^2)}} \tag{12}$$

where ε is a free parameter set to zero for a point mass.

Orbits inside the core. Fig. 2a shows the $(x, \dot{x})$ surface of section at the energy corresponding to $a=0.9r_c$ when $\mu=0$. Short-axis tube orbits generate the two bull's eyes while box orbits generate curves that encircle both bull's eyes. Most of the surface of section is occupied by box orbits. Fig. 2b shows the same surface of section when $\mu=0.02$ and $\varepsilon=0.07r_c$. One sees that the central object has transformed many box orbits into loops. (Quantitatively, loop orbits occupy 7 per cent of the total phase-space volume at this energy for $\mu=0$, and 42 per cent for $\mu=0.02$; see Section 5 for more details of phase-space volumes.) Little or no irregularity is evident. However, if we harden the Plummer model to $\varepsilon=0.05r_c$, irregularity starts to develop (Fig. 2c). When $\varepsilon\leqslant 0.03r_c$ the

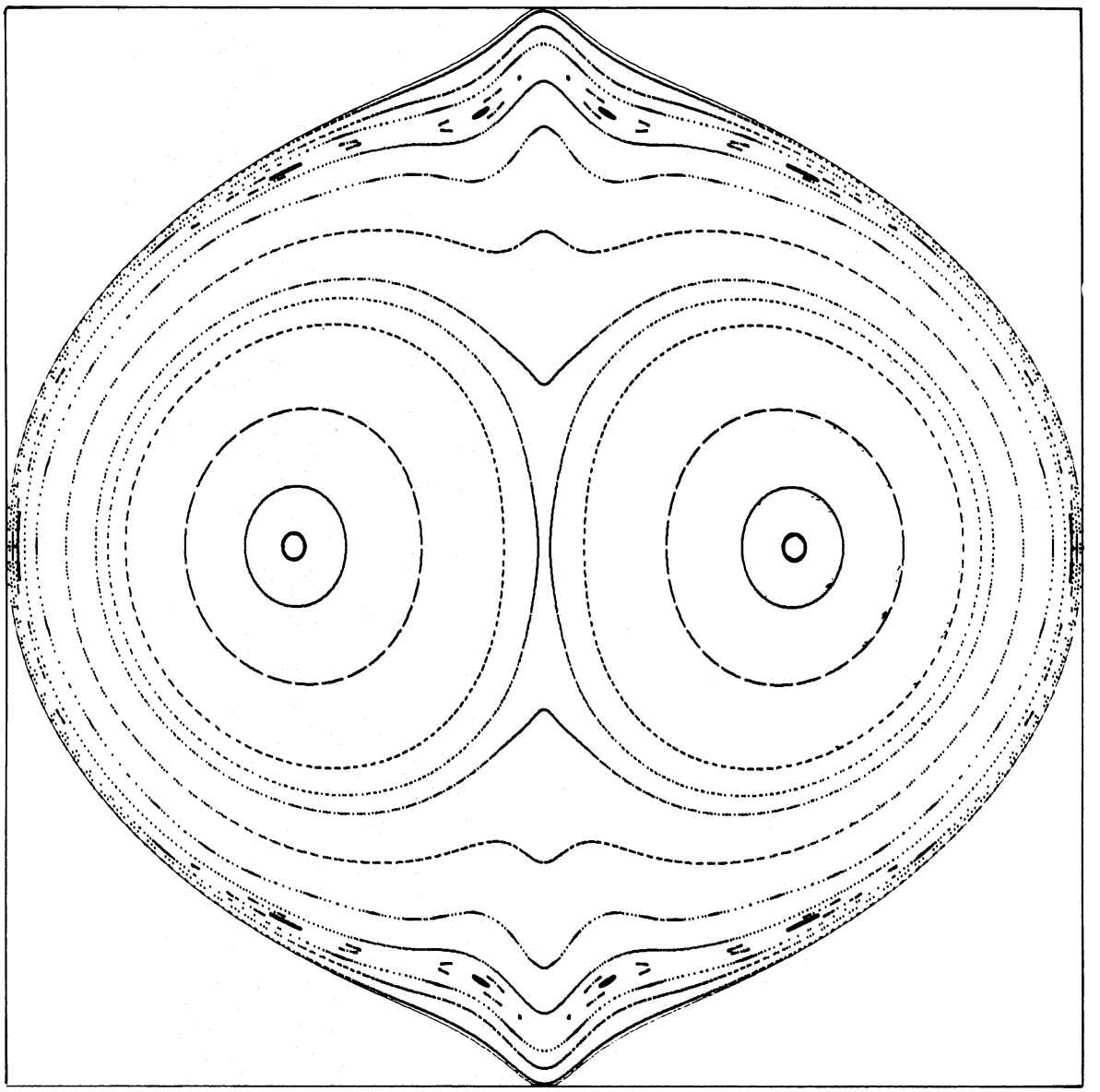

(b)

Figure 2 – *continued*

entire box region forms a single stochastic sea and an individual stochastic orbit fills the available area in the surface of section rather quickly. By equation (9) when $a=0.9r_c$ and $\mu=0.02$, the maximum impact parameter that leads to large-angle scattering by a point mass is $b_l=0.019r_c$. Since this is of the order of the softening radius ε at which most of the box orbits become irregular, this irregularity must be attributed to encounters with impact parameters equal to a few times b_l.

For $a=0.6r_c$ the situation is very similar. However, just outside the radius of influence of the central point mass ($r_h=0.27r_c$ for $\mu=0.02$), at $a=0.3r_c$, most orbits are either loops or belong to the resonant 2:1 family of 'banana' orbits (e.g. Binney 1982c).

Orbits outside the core. Fig. 3a and b show for $a=7r_c$ results equivalent to those shown in Figs 2a and b for $a=0.9r_c$. Since much of the surface of section is now occupied by loop orbits even when $\mu=0$, the introduction of a softened central object now alters the structure of the surface of section much less markedly than when $a=0.9r_c$. However, Fig. 4a shows that a point ($\varepsilon=0$) mass with $\mu=0.02$ seriously disturbs the box orbits. Several families of resonant orbits persist, but most of the area in the surface of section is again occupied by stochastic orbits.

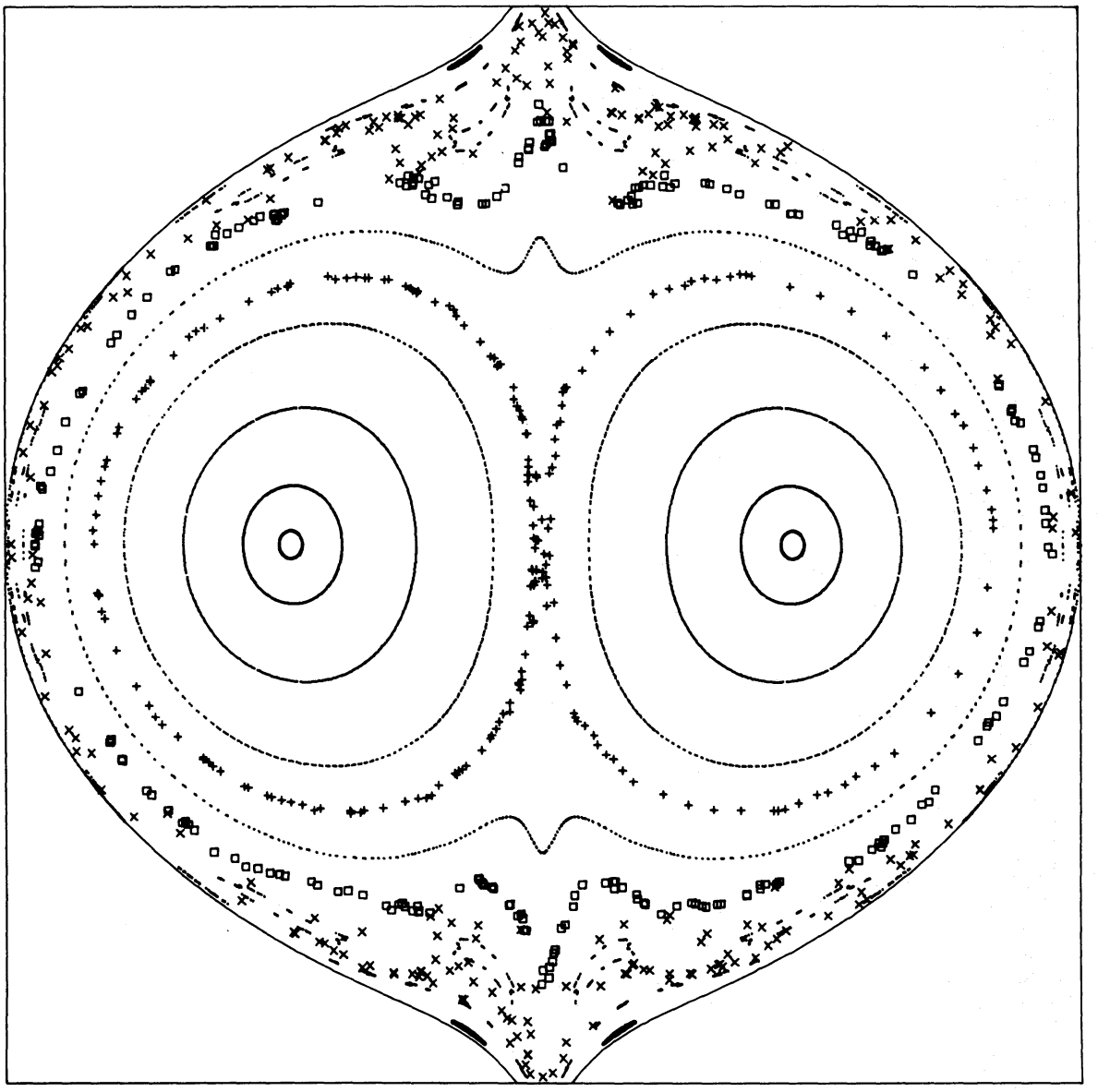

(c)

Figure 2 – *continued*

3.2.2 *Interpretation in terms of scattering*

We next investigate the relative importance of strong and weak encounters and the distribution of impact parameters with respect to the central mass. Figs 4b and c show the surfaces of section generated by two irregular orbits in the same potential as for Fig. 4a ($\mu=0.02$, $\varepsilon=0$). These surfaces of section contain about 50 points per orbit. The symbols marking the points change after the three closest passages past the centre. The respective impact parameters are $11b_l$, $5b_l$ and $2.5b_l$ in Fig. 4b, and $7b_l$, $0.8b_l$ and $11b_l$ in Fig. 4c. At the energy of these orbits, a hard encounter with the central object requires impact parameter $b<b_l=2.6\times10^{-3}r_c$. Figs 4b and c demonstrate the following:

(i) The computed orbits appear to be made up of a series of nearly regular segments, joined by discrete scattering events. The regular segments include segments of thin and fat box orbits, as well as highly eccentric loop orbits of either sense of rotation.

(ii) Fig. 4b shows an example of a hard ($b=2.5b_l$) encounter which dramatically changes the nature of the orbit, whereas Fig. 4c shows another ($b=0.8b_l$) which does not. The reason for this is presumably that at any spatial point a discrete set (usually four) of velocity vectors generate the same regular orbit. Clearly, if a star is scattered from one of these velocities to another, its orbit is unchanged.

(iii) Weak encounters can be important. The fact that a small scattering, for example that at $11b_l$ in Fig. 4c, can cause a star to move between very different orbits, shows the complexity of the perturbed phase space.

Fig. 5 shows the distribution of impact parameters for a number of stochastic orbits at three different energies for a central mass $\mu=0.02$. Here the impact parameter is determined as the star enters r_h, the radius of influence of the central object, or is taken as the minimum central distance when this is larger than r_h. Fig. 5a is based on approximately 150 core crossings per orbit, and confirms that the number of impacts with parameters less than b, $N(<b)$, rises approximately linearly with b as expected for a planar orbit. Slight variations exist between orbits of different energies, and even stochastic orbits at the same energy may differ from each other. In Fig. 5b one orbit has been integrated for a much longer time in order to resolve smaller impact parameters. At the energy of this orbit, $a=0.6r_c$, $b_l/b_{max}=2.1\mu r_c/b_{max}=0.21$. The fact that $N(<b)\propto b$ for these planar orbits down to less than b_l strongly suggests that correspondingly $N(<b)\propto b^2$ for three-dimensional box orbits. We shall lean heavily on this result in Sections 3.3 and 4.

As an additional check on our numerical integrations, and as a preliminary to the determination of the disruption time-scale for box orbits in the next subsection, we now show how one may understand the absolute values of $N(<b)$ in Fig. 5.

Estimating $N(<b)$ from the elapsed time and an argument like that on which equation (11) is based, assumes that the width of the waist of a box orbit is independent of energy. In the separable Stäckel potentials, box orbits are bounded by coordinate surfaces of a global coordinate system (de Zeeuw 1985a). Thin and thick boxes are bounded by different coordinate surfaces and so have different waists, but orbits enclosed by the same surfaces have central widths that are independent of energy. As a consequence of this, there is a maximum central width for box orbits of all energies, which turns out to be of order of the potential's core radius. In a non-separable potential like the potential (8) studied here, we no longer have a global coordinate system bounding the box orbits and the last two results no longer apply. In Fig. 6 we plot the width of the central waist r_w of box orbits in the logarithmic potential (8). r_w is largest for the fattest box orbits; we take its maximum value r_{wm} to be a factor $\sin 90°/\sin 60°=1.15$ larger than the value obtained for a box orbit of the same energy, but having corners on rays inclined at 60° to the long axis of the potential. (The exact value of r_{wm} is difficult to determine because orbits with corners near the potential's short axis are often irregular.)

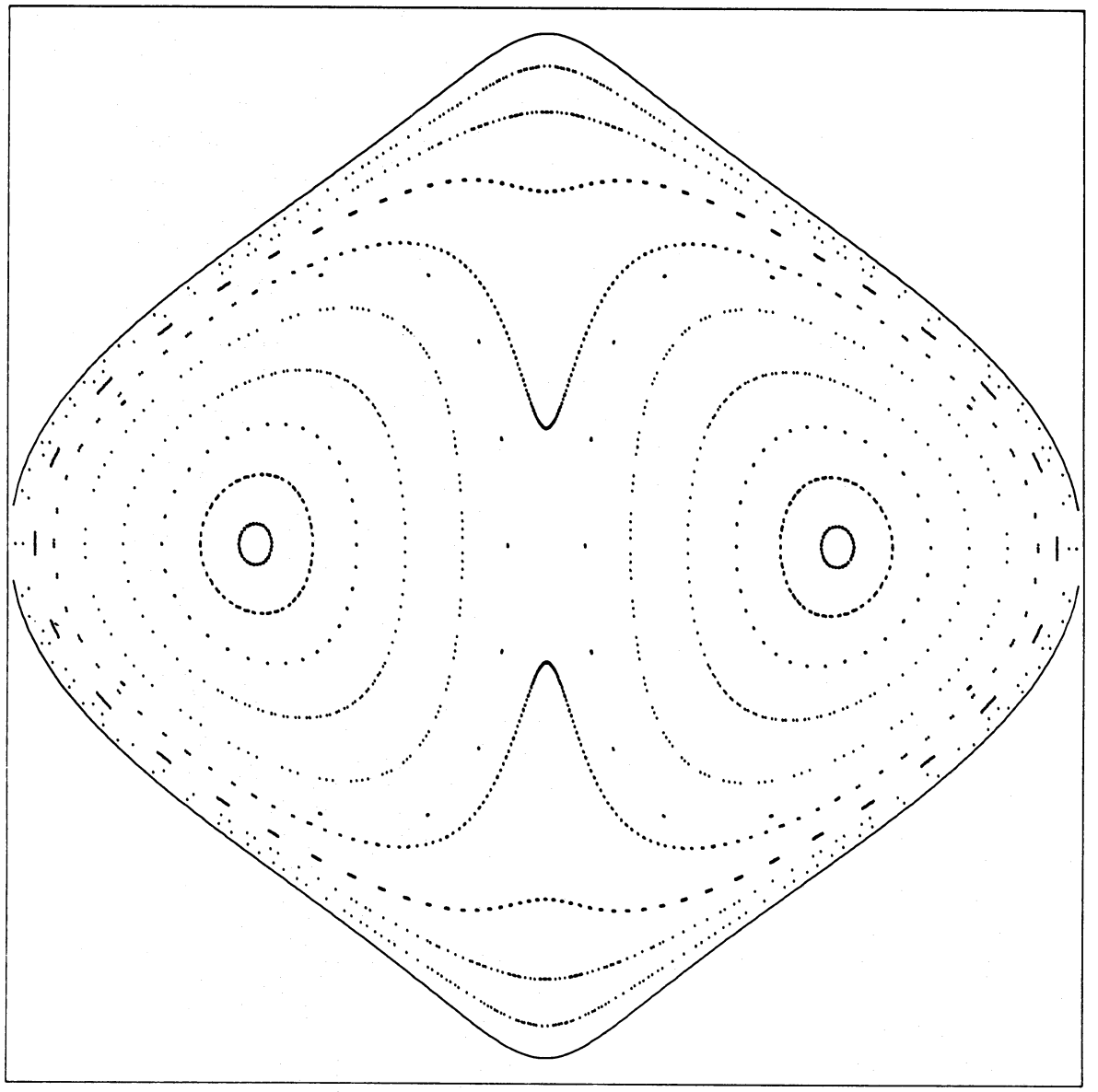

(a)

Figure 3. (a) $(x, \dot{x})$ surface of section as in Fig. 2a, but with $a=7r_c$. (b) as in (a), but with $\mu\simeq 0.02$ and $\varepsilon=0.01r_c$.

We have seen that box orbits in the presence of a central mass may be considered to be sequences of segments of unperturbed box orbits. Each segment is characterized by a different value of r_w. The star moves from one orbital segment to another after encountering the hole with impact parameter $b\leqslant 3b_l$. Hence on a given orbital segment we assume the probability of large-angle scattering to be

$$\frac{3b_l}{r_w} \tag{13}$$

per dynamical time. Repeated scattering will eventually establish a uniform distribution of stars within each element $d^2\mathbf{x}d^2\mathbf{v}$ of phase space that is accessible to box orbits of given energy E. If we replace $(\mathbf{x}, \mathbf{v})$ by the angle-action coordinates of these orbits, it is trivial to integrate over all orbital phases, and to conclude that after repeated scattering, the number of stars with energy E and different values of the angular action J_μ is proportional to dJ_μ/ω_r (Binney, Gerhard & Hut

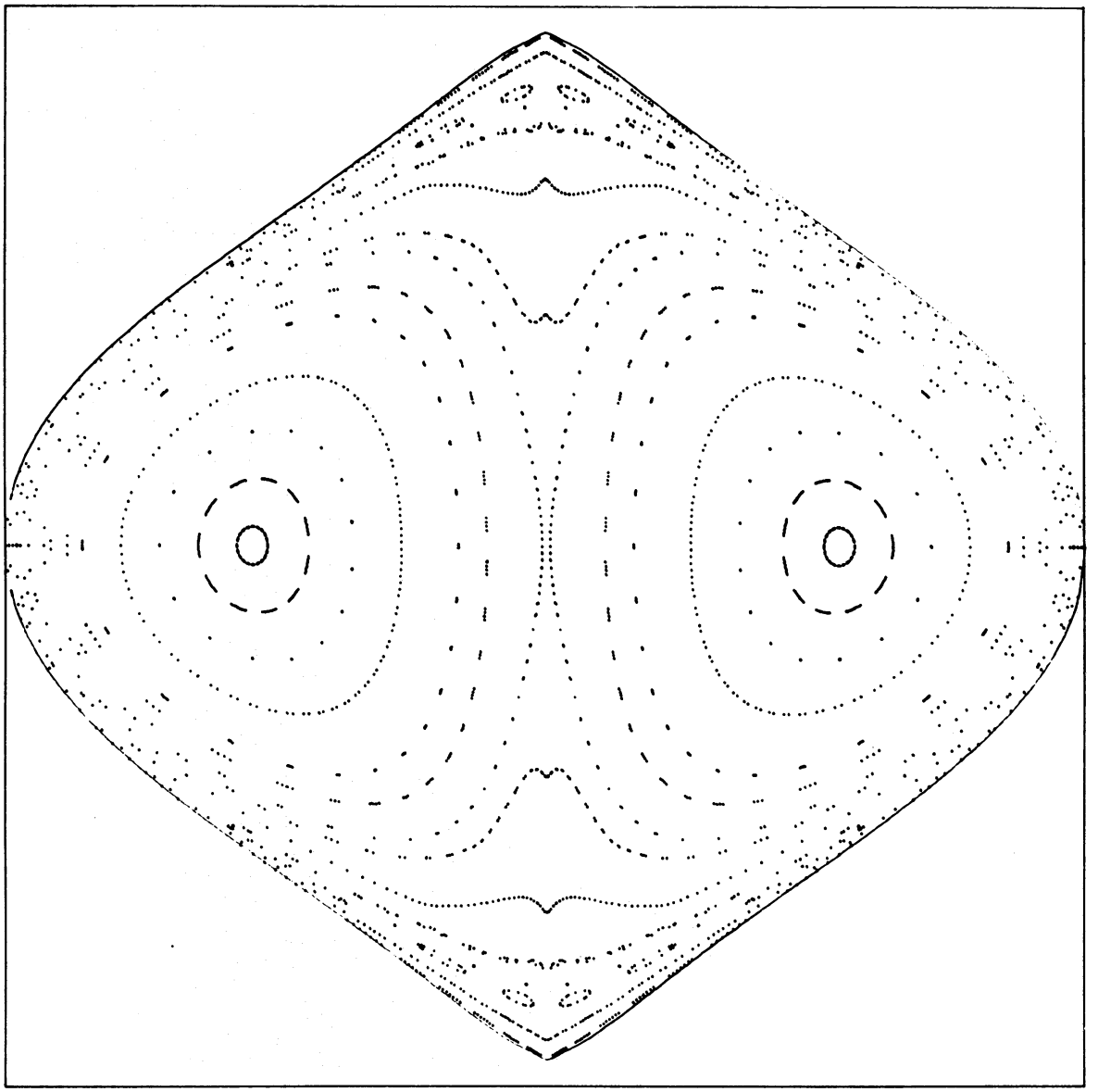

(b)

Figure 3 – *continued*

1985), where $\omega_r(E, J_\mu)$ is the radial frequency, and we follow de Żeeuw (1985a) in calling the relevant angular action J_μ. Hence we have that over a long period, the time spent by a given star on each orbital segment is

$$dt(r_w) \propto \frac{dJ_\mu(r_w)}{\omega_r} \propto r_w dr_w. \tag{14}$$

Here we have evaluated J_μ and μ_r in terms of r_w in the approximation that the motion is near-harmonic. Integrating the encounter rate with respect to t, we obtain for $r_{wm} > 3b_l$

$$N(<3b_l) = \frac{T}{\tau_{dyn}} \frac{\int_0^{3b_l} r_w dr_w + \int_{3b_l}^{r_{wm}} 3b_l dr_w}{\int_0^{r_{wm}} r_w dr_w} \simeq \frac{6b_l}{r_{wm}} \frac{T}{\tau_{dyn}} \tag{15}$$

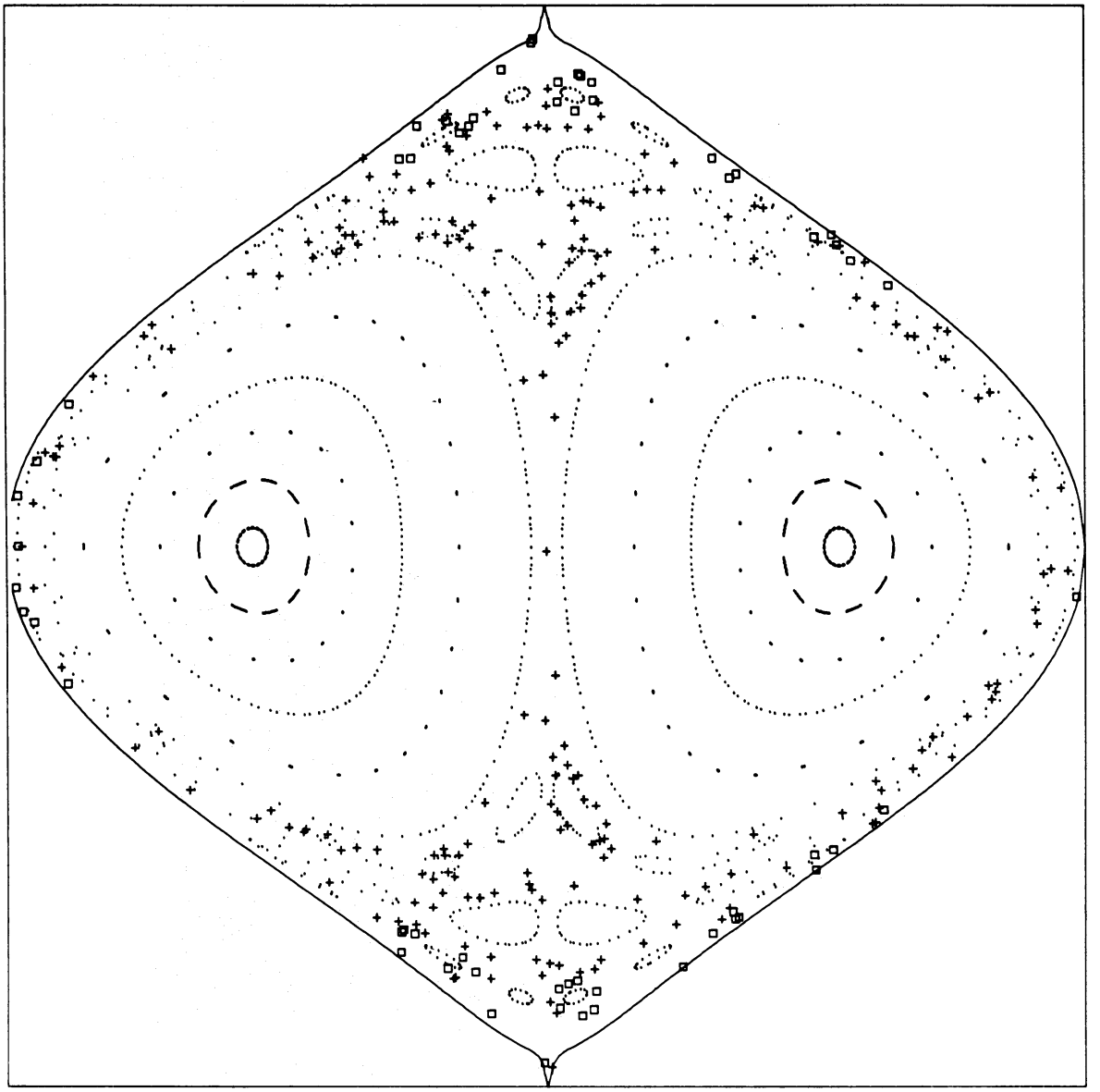

(a)

Figure 4. (a) $(x, \dot{x})$ surface of section as in Fig. 2, but for $a=7r_c$ and a point mass ($\mu=0.02$, $\varepsilon=0$). Loop orbits and resonant orbits (dots) are separated by stochastic regions, in which points generated by distinct orbits are marked by different symbols. (b) The history of a single irregular orbit as in (a) but for $\mu=0.02$. The star is initially on a double-loop orbit (+). An encounter at $11b_l$ does not alter the orbit's nature (∇), but it becomes a fat box orbit after a $5b_l$ encounter with the centre (×). It converts to a thin box after a $2.5b_l$ encounter ($\Diamond$). (c) History of a second stochastic orbit as in (b). Initially a box (+), it shifts to a different box (∇) after a $7b_l$ encounter, changes very little after a $0.8b_l$ encounter (×), and finally moves to a double-loop orbit after an $11b_l$ encounter ($\Diamond$).

where T is the total time interval considered. For the orbits with $a=(0.6r_c, 0.9r_c, 7r_c)$ plotted in Fig. 5, we find $N(<3b_l)=(100, 52, 2.2)$. This is in excellent agreement with the empirical values (116, 52, 3). In fact, for the lowest energy orbits, the agreement must be considered partly fortuitous, since such orbits are dominated by the hole much of the time.

3.2.3 Summary of the numerical results

(i) When a point mass with about 2 per cent of the galaxy's core mass is placed at the centre of the galaxy, box orbits at low and intermediate energies become highly stochastic. Inside the core

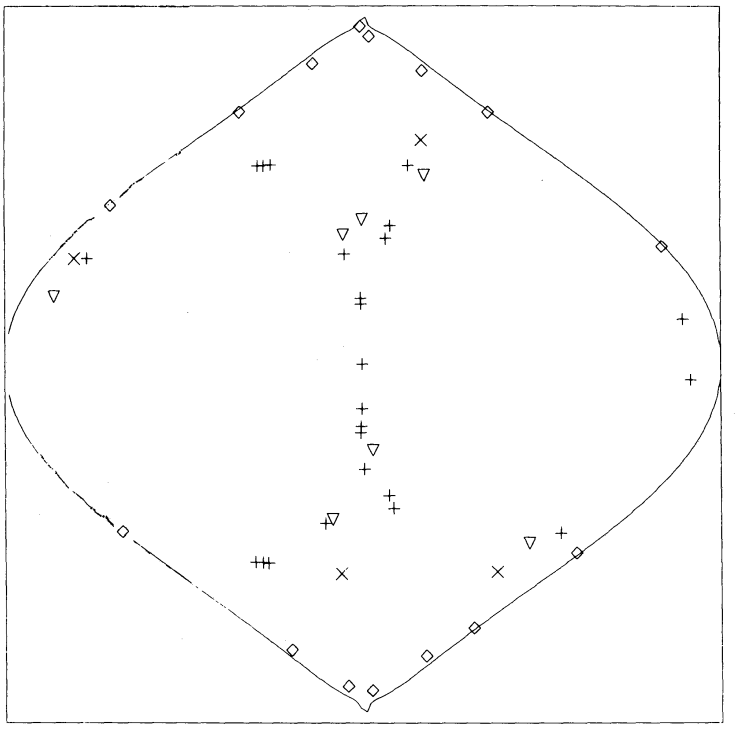

(b)

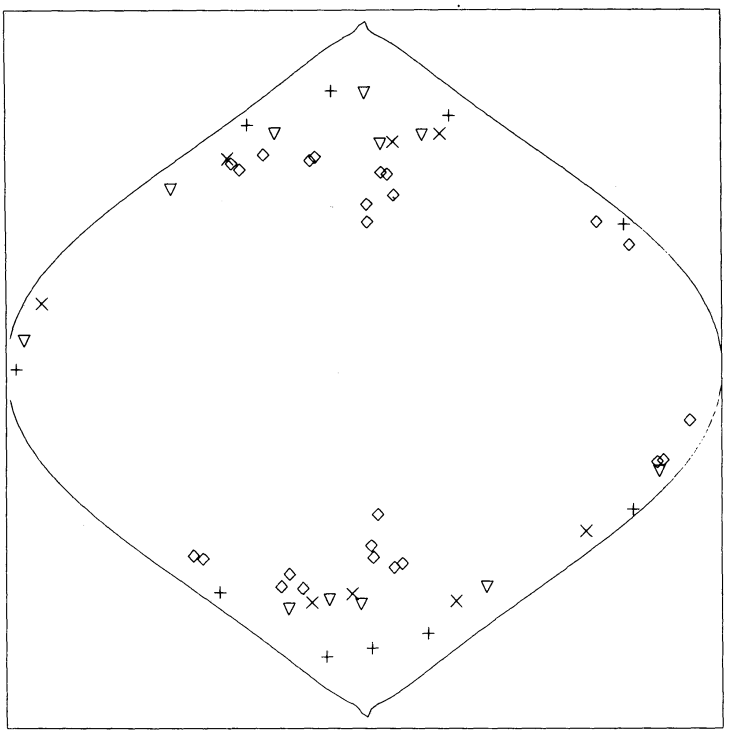

(c)

Figure 4 – *continued*

radius, some box orbits are transformed into loops, but most become stochastic. Only a small fraction of the box orbits reaching out to several galaxy core radii avoid disruption by being trapped in orbital resonances.

(ii) Irregular orbits at energies corresponding to several core radii can be described as sequences of segments of regular box orbits.

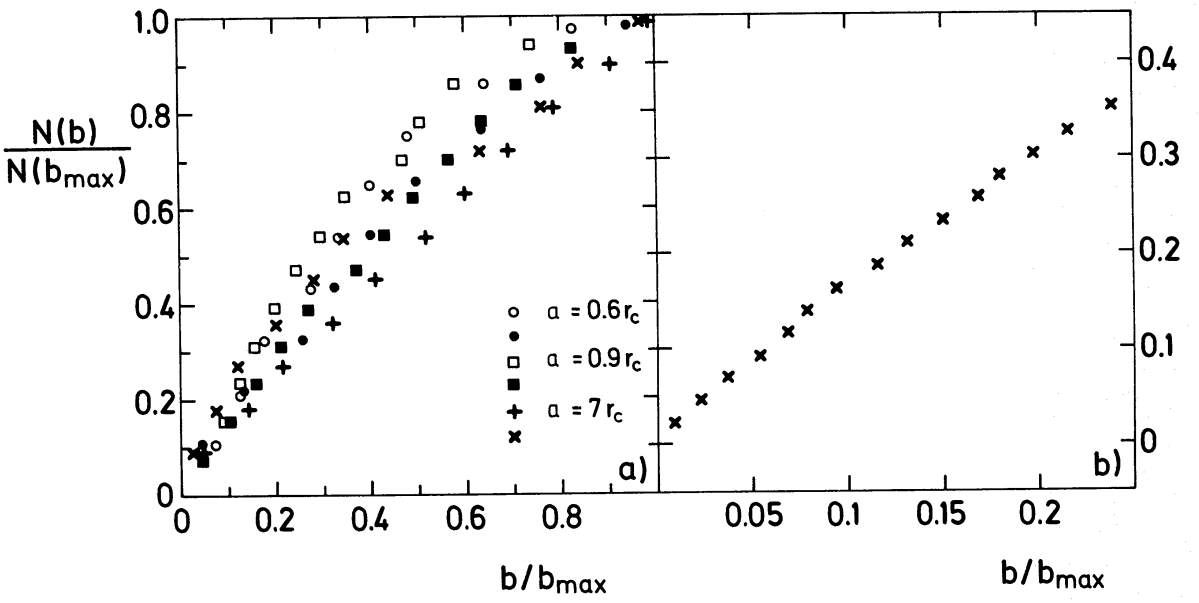

Figure 5. Distribution of impact parameters for orbits of several energies in the logarithmic potential (8) and a point mass $\mu = 0.02$. Results are shown for two orbits at each energy.

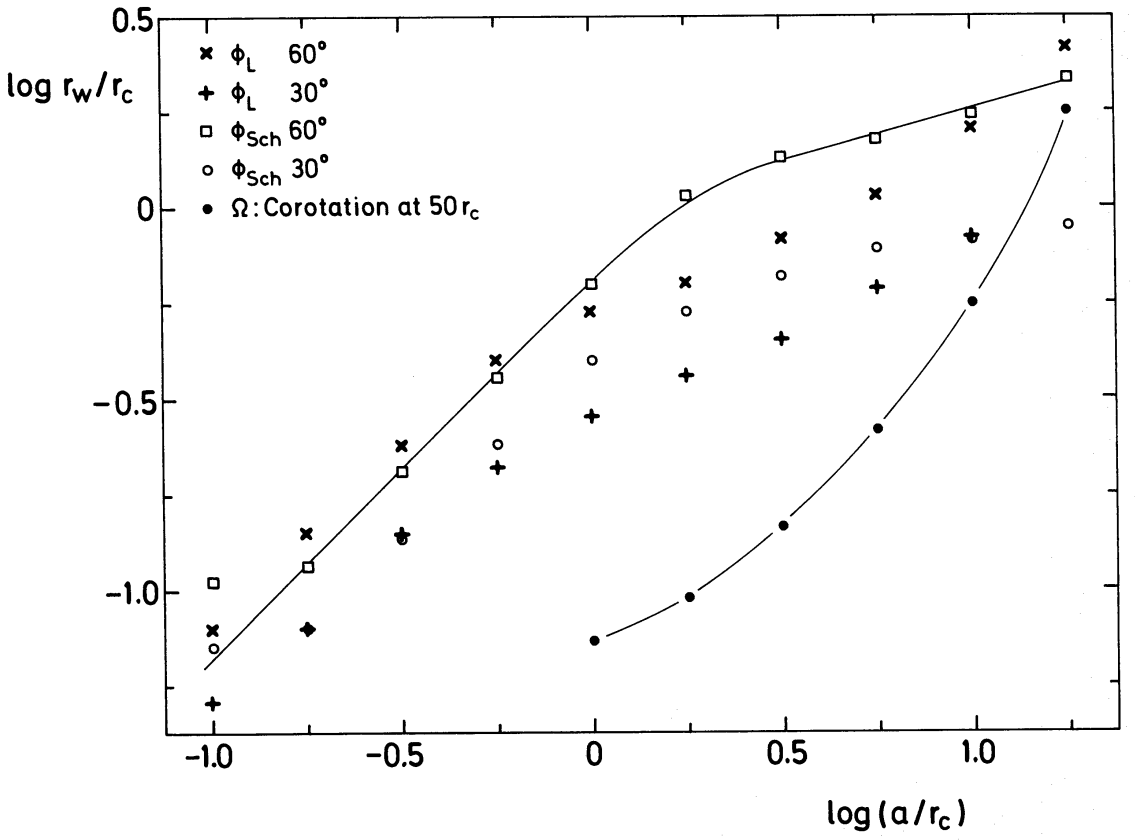

Figure 6. The width of the central waist of box orbits and the effect of rotation. Φ_L is the potential defined by equation (8), while Φ_{Sch} is the de Zeeuw & Merritt (1983) approximation to Schwarzschild's (1979) potential. The filled circles show, for orbits in a rotating potential of the form (8), the quantity y_0 defined in the text.

(iii) Encounters with the central object closer than about $3b_l$ give rise to transitions between orbital segments.

(iv) In the planar case, all impact parameters up to the width r_w of the waist of a given segment are equally probable.

3.3 TIME-SCALE FOR DISRUPTION OF 3-DIMENSIONAL BOX ORBITS

In the last subsection, we analysed planar box orbits in the combined potential of a central black hole and the logarithmic model (8), and concluded that these orbits can be understood in terms of simple scattering by the hole. We found that although weak encounters contribute to the evolution of a typical orbit, the dominant contribution to any orbit's evolution seems to come from encounters at $b<3b_l$. Since a general three-dimensional box orbit may be thought of as a development of a planar orbit like those discussed in the last subsection, it is likely that three-dimensional box orbits in the presence of a hole can likewise be understood as box orbits that are repeatedly scattered by the hole. Moreover, although in three dimensions weak encounters are relatively more numerous than in two, and one might be concerned that the cumulative effect of weak encounters might exceed that of encounters at $b<3b_l$, it seems likely that in three dimensions close encounters still dominate because (i) the half-width of the waist of any orbital segment imposes a clear upper limit on the impact parameters that need be considered, and (ii) our experiments with softened central objects suggest that distant encounters are ineffective generators of irregularity. Therefore we now use our picture of orbital evolution powered by encounters at $b<3b_l$ to estimate the time-scale for disruption by a central hole of the three-dimensional box orbits of a triaxial galaxy.

For definiteness we use Schwarszchild's (1979) potential. The density distribution that generates this potential is constant on similar concentric ellipsoids with axis ratios 1:0.625:0.5. The density on each ellipsoid depends on the ellipsoid's semi-major axis length in the same way as the density of the modified Hubble model,

$$\varrho(r)=\varrho_0\left\{1+\left(\frac{r}{r_c}\right)^2\right\}^{-3/2} \tag{16a}$$

depends on radius r. Hence the monopole component of Schwarzschild's potential is approximately

$$\Phi(r)=-9\sigma_0^2\left(\frac{r_c}{r}\right)\ln\left[\frac{r}{r_c}+\left\{1+\left(\frac{r}{r_c}\right)^2\right\}^{1/2}\right], \tag{16b}$$

where we have used King's (1962) approximate formula

$$\varrho_0\simeq\frac{9\sigma_0^2}{4\pi G r_c^2} \tag{16c}$$

to eliminate ϱ_0 in favour of the central velocity dispersion σ_0. The core mass (equation 5) of this model is

$$M_c=1.57\,\frac{r_c\sigma_0^2}{G}. \tag{16d}$$

Thus the impact parameter b_l for large-angle deflection may be written (see equation 7)

$$b_l=\frac{G\mu M_c}{2\{\Phi_G(a)-\Phi_G(r_h)\}}\simeq 0.73\frac{\mu r_c}{f(\alpha)}, \tag{17}$$

where

$$f(\alpha)\equiv 8.4\left[1-\frac{\ln\{\alpha+\sqrt{(1+\alpha^2)}\}}{\alpha}\right] \tag{18}$$

is chosen such that $f(1)=1$. Here α is the dimensionless orbital amplitude $\alpha\equiv a/r_c$, and equations (17) apply only for $a>r_h$, $r_h\ll r_c$. Finally, the dynamical time in this model is

$$\tau_{dyn}(a)=2\left[\frac{a^3}{GM(a)}\right]^{1/2}=\frac{2}{3}\frac{r_c}{\sigma_0}\left[\frac{\alpha^3}{\ln\{\alpha+\sqrt{(1+\alpha^2)}\}-\alpha/\sqrt{(1+\alpha^2)}}\right]^{1/2}. \tag{19}$$

For small orbital amplitudes a, $\tau_{dyn}(a)=2r_c/(\sqrt{3}\sigma_0)$ as expected for an isothermal core, and for large a, $\tau_{dyn}(a)\simeq(2r_c/3\sigma_0)\sqrt{(a^3/\ln\alpha)}$ increases faster than in an isothermal sphere $\{\tau_{dyn}(a)\propto a\}$ because of the more rapidly falling density profile.

The plane $x=0$ cuts the waist of a three-dimensional box orbit in an approximately rectangular region. So if, by analogy with the planar case, at any passage through $x=0$ all impact parameters in the rectangle ($|y|<y_w$, $|z|<z_w$) are equally likely, and we have no prior information about the orbital phase, the expectation value of the time to first scattering on a given orbit is

$$\tau_1(y_w, z_w; a)=\frac{4y_w z_w}{\pi(3b_l)^2}\tau_{dyn}(a). \tag{20}$$

We obtain the mean time to first encounters for all stars on box orbits of a given energy by averaging τ_l over y_w and z_w. Let the galaxy have distribution function $f(E, J_\mu, J_\nu)$ depending on energy and the two angular actions J_μ and J_ν. Then

$$\tau_{dis}(a)=\frac{\int f\tau_l dJ_\mu\, dJ_\nu}{\int f dJ_\mu\, dJ_\nu}. \tag{21}$$

By analogy with the three-dimensional harmonic oscillator, we assume $J_\mu\propto y_w^2$, $J_\nu\propto z_w^2$ and integrate over the rectangular region of the (J_μ, J_ν) plane ($y_w\leq r_{wm}$, $z_w\leq r_{wm}$). In the absence of any knowledge of the distribution function we take f to be the step function,

$$\begin{aligned} f &= f_0 \quad (y_w<\tfrac{1}{2}r_{wm},\ z_w<\tfrac{1}{2}r_{wm}),\\ &= 0 \quad \text{otherwise.}\end{aligned} \tag{22}$$

Then

$$\tau_{dis}(a)=\frac{4}{81\pi}\left(\frac{r_{wm}}{b_l}\right)^2\tau_{dyn}(a). \tag{23}$$

We assume $r_{wm}\simeq 1.15\, r_w(60°)$ as above, where $r_w(60°)$ is the width of the waist of the planar orbit started by releasing a star in de Zeeuw & Merritt's (1983) approximation to Schwarzschild's potential* from the intersection of the zero-velocity curve and a line inclined at 60° to the x-axis. Fig. 6 shows $r_w(60°)$ and $r_w(30°)$ as functions of orbital scale a. One sees that the restriction of f to $(y_w, z_w)<\frac{1}{2}r_{wm}$ corresponds to allowing only orbits with opening angles smaller than 30°. An approximate fit to r_{wm} is

$$r_{wm}(a)\simeq 0.76a\left\{1+\left(\frac{a}{1.8r_c}\right)^{3.75}\right\}^{-1/5}. \tag{24}$$

*The value of c_4 given by de Zeeuw & Merritt (1983) is in error. The correct value is $c_4=0.48068$.

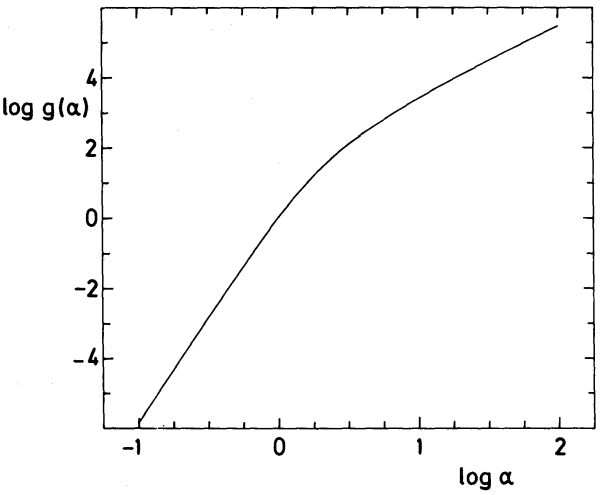

Figure 7. The dimensionless function $g(\alpha)$.

While the increase of $r_{\rm wm}$ for $a>r_{\rm c}$ is purely empirical, arising from the non-separable nature of Schwarzschild's potential, the dependence $r_{\rm wm}\propto a$ for $a<r_{\rm c}$ is a consequence of the shrinking zero-velocity curve inside $r_{\rm c}$ being essentially filled by the Cartesian box orbit.

Equation (23), with equations (17), (19) and (24), now yields

$$\tau_{\rm dis}\simeq 6.4\times 10^{7}\left(\frac{\mu}{0.02}\right)^{-2}\left(\frac{r_{\rm c}}{240\,{\rm pc}}\right)\left(\frac{\sigma_0}{240\,{\rm km\,s^{-1}}}\right)^{-1} g(\alpha)\,{\rm yr} \tag{25a}$$

where $g(\alpha)$ is the dimensionless function plotted in Fig. 7. $g(\alpha)$ rises rapidly inside the core $\alpha<1$, to $g(1)=1$, and has asymptotic behaviour $g(\alpha)\propto\alpha^2$ for large α. Again there is a critical mass $\mu_{\rm dis}(a)$ capable of destroying most box orbits with apocentres at $a'<a$ in 10^{10} yr: for example, for the typical core parameters given above, $\mu_{\rm dis}(r_{\rm c})\simeq 1.6\times 10^{-3}$. However, the steep rise of $g(\alpha)$ at large α protects the high-energy box orbits; for $\mu=0.02$, $t_{\rm dis}=10^{10}$ yr for $a=3.5r_{\rm c}$, and even for $\mu=0.1$ only orbits out to $12r_{\rm c}$ are affected by scattering. High-energy box orbits can therefore only know of a central massive body indirectly, through the collective changes in the core. A useful alternative form of equation (25a) gives the scale $a_{\rm dis}$ out to which scattering by a black hole of mass m has been effective up to the present epoch;

$$a_{\rm dis}\simeq 500\left(\frac{m}{10^{8}\,M_{\odot}}\right)\left(\frac{r_{\rm c}}{240\,{\rm pc}}\right)^{-1/2}\left(\frac{\sigma_0}{240\,{\rm km\,s^{-1}}}\right)^{-3/2}{\rm pc}\qquad (a_{\rm dis}>5r_{\rm c}). \tag{25b}$$

3.4 FIGURE ROTATION OF THE POTENTIAL

As was discussed in Section 2, the figures of elliptical galaxies can rotate slowly if at all. However the spheroids of disc galaxies may be tumbling triaxial systems, so it is of interest to enquire how our conclusions are affected by rotation of the figure of the potential.

We assume that the potential rotates about its smallest principal axis. The closed long-axial orbits that are the parents of the all-important box [or 'x_1 orbits' in the notation of Contopoulos & Papayannopoulos (1980)] are then prograde orbits which no longer pass through the exact centre of the galaxy. The distance y_0, at which these orbits pass the centre as they cross the intermediate axis of the potential, increases with orbital energy and with the angular speed ω at which the potential rotates; y_0 becomes comparable to the orbit's scale a as a approaches the corotation radius $a_{\rm corot}$.

Clearly, if a substantial fraction of the box orbits of scale a never come within b_l of the centre, a self-consistent bar of that scale may persist indefinitely. This condition will be approximately satisfied if $y_0 \geqslant r_{\rm wm}$, where $r_{\rm wm}(a)$ is the maximum central width of a box orbit in the absence of figure rotation or black hole. y_0 is plotted in Fig. 6 for the logarithmic potential (8) and an angular speed ω that places $a_{\rm corot}$ at $50r_{\rm c}$. It is clear that while figure rotation is capable of preserving box orbits with scales $a > 10r_{\rm c}$, i.e. orbits that reach out to at least a quarter of the corotation radius, it cannot prevent the dissolution of box orbits in the core of the galaxy.

4 Effect of orbit disruption on the galaxy and the hole

Two important questions are raised by the possibility that black holes sometimes form at the centres of triaxial spheroidal components:

(i) How does triaxiality of the spheroid affect the rate at which the hole is fed with material that it can accrete?

(ii) Is the spheroid's triaxiality ultimately destroyed by the growth of the hole?

These questions were discussed by Norman & Silk (1983) and by Lake & Norman (1983), but the results of the last section enable us to give a more satisfactory treatment of these questions here.

4.1 DESTRUCTION OF TRIAXIALITY

In Sections 2 and 3 we have argued that in the absence of significant figure rotation, a stellar system can be triaxial only if at most energies, the phase-space density of stars is highest in the portion of phase space occupied by the box orbits. Moreover, since it is only the more elongated box orbits which support the bar, a self-consistent system can be triaxial only if in it these orbits are considerably more heavily populated than the fatter boxes.

By scattering stars on box orbits, a central massive object will tend to establish a uniform distribution of stars amongst all box orbits. As the fatter box orbits are populated at the expense of the elongated box orbits, the galaxy's potential becomes rounder. This has the effect of making all box orbits, at given actions, fatter, and of converting some of the fattest box orbits into tube orbits, which always oppose the galaxy's bar. Furthermore, as the galactic potential evolves some orbits are first trapped into and then released from families of resonant box- and tube orbits (Binney & Spergel 1984), with the overall effect of further homogenizing the stellar distribution over orbits. Hence scattering of stars on box orbits must eventually lead to the breakdown of triaxiality.

What is less certain is whether the destruction of triaxiality occurs abruptly in the manner of a phase change, or proceeds at a steady and unspectacular rate. The possibility of a steady change arises because $\tau_{\rm dis}(a)$ is a rapidly increasing function of a. Hence, in a fixed potential, the smaller box orbits are disrupted much before the larger ones and axisymmetry may spread gradually from the centre as the dissolution of box orbits of each scale a approaches completion. Alternatively, the onset of axisymmetry may occur abruptly because, in a self-consistent system, the early disruption of the small box orbits so undermines the triaxiality of the potential that the larger box orbits immediately convert to tube orbits, and the galaxy becomes axisymmetric forthwith.

Clearly, orbit integrations in a given potential such as we present here, do not suffice for a definitive determination of whether the onset of axisymmetry is gradual or abrupt. At some stage n-body models may be able to settle this question, but recent work by Norman, May & van Albada (1985) indicates that individual orbits in n-body models are currently not integrated with sufficient accuracy for one to have confidence in results obtained with triaxial n-body systems containing massive central objects. However, the following simple calculation strongly suggests

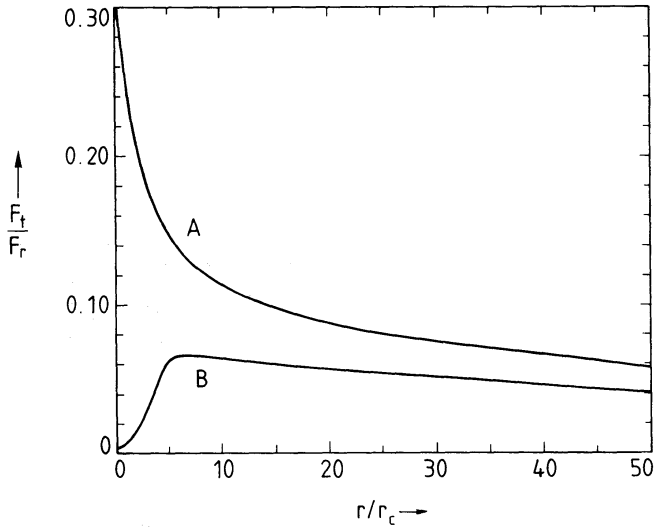

Figure 8. The ratio F_t/F_r of the tangential to the radial force on a star as a function of distance a down a line inclined at 45° to the long axis of prolate hubble-type body with axis ratios $a:b:c$ equal to (A) 1:0.6:0.6 and (B) as specified by equation (26).

that triaxiality will be lost gradually, from the centre outwards, rather than suddenly in the manner of a phase change.

Fig. 8 shows the ratio F_t/F_r of the tangential to the radial forces on stars in two prolate galaxies when the stars lie along lines inclined at 45° to the major axes of the systems. Since it is the tangential force F_t which every few dynamical times reverses the angular momentum of stars on box orbits, the ratio F_t/F_r at radius a is likely to be a good indicator of the fraction of orbits with apocentres near a which are box orbits. Hence the destruction of triaxiality in the core is likely to undermine the triaxiality further out only if the adoption of a spherical shape by the core significantly diminishes the tangential force F_t further out. One of the systems of Fig. 8, system A, has at all radii axis ratios 1:0.6:0.6 similar to those (1:0.625:0.5) of Schwarzschild's model. One sees that for this system F_t/F_r rises from 11 per cent at 10 core radii to 30 per cent in the core, in line with the increase in the box orbit fraction (see Fig. 10). The second system for which F_t/F_r is plotted in Fig. 8, system B, has axis ratios $1:q(a):q(a)$, where

$$q(a)=1-0.2\left\{\tanh\left(\frac{a/r_c-5}{1.5}\right)+1\right\}. \tag{26}$$

Hence, in system B, $q(a)\simeq 1$ for $a\leqslant 3.5r_c$, and $q(a)\simeq 0.6$ for $a>6.5r_c$. Now F_t/F_r rises from 6.3 per cent at $10r_c$, to 6.5 per cent at $5.5r_c$ and then falls roughly linearly with a to less than 0.4 per cent in the core.* Thus allowing the core to become spherical, as in system B, has little effect on the triaxiality of the potential further out. This suggests that at time $t=\tau_{dis}(a)$, a triaxial galaxy will approach axisymmetry at radii $r<a$, and be markedly triaxial at $r>a$.

If triaxiality really is lost gradually, triaxial galaxies with central massive objects should *tend* to appear rounder near their centres than further out. The work of Di Tullio (1979), Lauer (1985) and others suggests that many giant ellipticals have such ellipticity profiles. However, it should be borne in mind that at certain projection angles, the reverse effect will be observed, so this prediction is intrinsically of a statistical nature.

* It is perhaps worth noting that $F_t(10r_c)$ in system B equals $0.971\times F_t(10r_c)$ in system A; at $10r_c$, F_t/F_r is significantly smaller in system B only because this system has more matter at small radii.

4.2 FEEDING THE MONSTER

A star of mass m^* and radius r^* will be tidally disrupted if it comes within radius

$$r_t = 2(m/m_*)^{1/3} r_* \simeq 2.1\times10^{-5}\left(\frac{m}{10^8\,M_\odot}\right)^{1/3}\ \mathrm{pc} \tag{27}$$

of a nucleus of mass m. We assume that the central mass accretes all the material of shredded stars, and hence grows at a rate equal to the rate at which stars come within r_t of the galaxy centre.

Clearly many stars are on orbits that do not carry them within r_t of the centre. This is most easily understood in the case of an axisymmetric galaxy, when only stars with angular momenta

$$L<L_t\equiv r_t v = r_t\left[\frac{2Gm}{r_t}+2\{E-\Phi_0(r_t)\}\right]^{1/2}\simeq(2Gmr_t)^{1/2} \tag{28}$$

come closer than r_t. In the case of a triaxial galaxy, a similar condition applies; only the box orbits and the most eccentric long- and short-axis tube orbits pass close to the nucleus, and the condition (28) is replaced by similar conditions on the angular actions J_μ and J_ν that take the place of angular momentum for orbits in a non-rotating triaxial potential. However, we are not simply interested in how many stars are *in principle* subject to shredding by a central hole: we need to know the rate at which the hole shreds stars. Here there is a sharp distinction to be drawn between the axisymmetric and the triaxial cases.

In the axisymmetric case only a very small proportion of the phase space at most energies is associated with orbits that expose stars to shredding, and these orbits carry stars past the hole once per orbital time. Consequently these orbits are soon depopulated, and the hole subsequently feeds only as fast as collisional processes scatter stars on to the depopulated orbits (Frank & Rees 1976; Lightman & Shapiro 1977). In the triaxial case, by contrast, a large proportion of the phase space at all energies is associated with orbits that expose stars to shredding, and these orbits may well carry the bulk of the mass of the entire galaxy (Schwarzschild 1979). However, stars on these orbits pass within r_t of the hole much more rarely that once per dynamical time. Hence the hole may be expected to feed on the bulk of the galactic mass, but only over many galactic dynamical times.

For a star of given energy, or equivalently of the ratio $\alpha=a/r_c$, there is evidently a minimum impact parameter b_t at which the star can enter the region of radius r_h within which the hole dominates the net gravitational force-field, and yet escape shredding by the hole. If

$$v_h\simeq[2\{\Phi_G(a)-\phi_G(r_h)\}]^{1/2}$$

is the speed of the star at r_h, energy and angular momentum conservation for this critical trajectory yield for $2Gm/r_t \gg v_h^2 > 2Gm/r_h$,

$$b_t=\frac{(2Gmr_t)^{1/2}}{v_h}\simeq0.011\left(\frac{400\ \mathrm{km\ s^{-1}}}{v_h}\right)\left(\frac{m}{10^8\,M_\odot}\right)^{2/3}\ \mathrm{pc}\gg r_t. \tag{29}$$

We saw in Section 3 that the hole tends to disrupt box orbits after a time t_{dis} of the order of that required for the star to encounter the hole with impact parameter smaller than three times the value b_l given by equation (7). Clearly, if $b_l \gg b_t$, the majority of box orbits will be disrupted by the hole before the stars on them have been shredded. Eliminating Gm/v_h^2 between equations (7) and (29), we have

$$\frac{b_t}{b_l}\simeq\frac{2r_t}{b_t}. \tag{30}$$

Hence $b_t \ll b_l$, and only a small fraction $\simeq (b_t/b_l)^2$ of stars on vulnerable orbits are captured before their orbits are disrupted.

If the hole accretes all the matter of shredded stars, its mass m grows at a rate

$$\frac{dm}{dt} \simeq \int_0^{E_{\rm dis}} \left(\frac{b_t}{3b_l}\right)^2 \frac{dM}{dE} \frac{dE}{\tau_{\rm dis}(E)}, \tag{31}$$

where $E_{\rm dis}(t)$ is the energy of box orbits for which $\tau_{\rm dis}=t$, and $M(E)$ is the mass in stars with energies $E'<E$. Binney & Petrou (1985) show that $M(E)$ is largely determined by the radial density profile of the galaxy. Hence an accurate estimate of $M(E)$ for Schwarzschild's model may be obtained by using Eddington's (1916) formula for the distribution function $f(E)$ that

Table 1. Dynamical quantities for a system with density $\varrho=[1+r^2\{1+(r/100)^2\}]^{-3/2}$. For $r<70$ this system has the same radial profile as Schwarzschild's model. The fourth column gives $E=|\Phi(r)|$, the fifth the value of the self-consistent distribution function, and the third the total mass on orbits with binding energies $E'>E$. The sixth and seventh columns give estimates for Schwarzschild's model of the time-scales (19) and (23) when this model is scaled to $r_c=240$ pc, $\sigma_0=240$ km s^{-1}. The last column gives the accretion rate from equation (31) for a $10^8\,M_\odot$ black hole at the centre of Schwarzschild's model scaled thus. The values of $\tau_{\rm dis}$ given in column 7 are slightly more accurate than those given by equation (25a).

$\log r$	$M(r)$	$M(E)$	E	$f(E)$	$\tau_{\rm dyn}$/yr	$\tau_{\rm dis}$/yr	$M/(M_\odot\,{\rm yr}^{-1})$
−1.0	4.15E−03	1.62E−06	1.23E+01	3.70E−02	1.14E+06	1.14E+06	
−0.9	8.24E−03	3.42E−06	1.23E+01	3.71E−02	1.14E+06	1.14E+06	
−0.8	1.63E−02	1.86E−05	1.23E+01	3.69E−02	1.14E+06	1.14E+06	
−0.7	3.21E−02	9.66E−05	1.22E+01	3.61E−02	1.15E+06	1.15E+06	
−0.6	6.28E−02	4.31E−04	1.22E+01	3.49E−02	1.16E+06	1.16E+06	
−0.5	1.22E−01	1.72E−03	1.21E+01	3.32E−02	1.18E+06	1.18E+06	1.10E−04
−0.4	2.31E−01	6.33E−03	1.20E+01	3.05E−02	1.21E+06	1.21E+06	1.09E−04
−0.3	4.30E−01	2.14E−02	1.19E+01	2.69E−02	1.25E+06	1.25E+06	1.04E−04
−0.2	7.74E−01	6.61E−02	1.16E+01	2.25E−02	1.32E+06	3.11E+06	8.65E−05
−0.1	1.34E+00	1.82E−01	1.13E+01	1.76E−02	1.42E+06	1.34E+07	6.65E−05
0.0	2.19E+00	4.45E−01	1.08E+01	1.28E−02	1.57E+06	5.13E+07	4.83E−05
0.1	3.39E+00	9.55E−01	1.03E+01	8.59E−03	1.78E+06	1.77E+08	3.35E−05
0.2	4.97E+00	1.81E+00	9.60E+00	5.43E−03	2.07E+06	5.43E+08	2.26E−05
0.3	6.88E+00	3.05E+00	8.84E+00	3.27E−03	2.49E+06	1.47E+09	1.49E−05
0.4	9.08E+00	4.68E+00	8.03E+00	1.91E−03	3.06E+06	3.48E+09	9.78E−06
0.5	1.15E+01	6.64E+00	7.19E+00	1.10E−03	3.84E−06	7.49E+09	6.33E−06
0.6	1.41E+01	8.87E+00	6.36E+00	6.31E−04	4.90E+06	1.50E+10	4.06E−06
0.7	1.67E+01	1.13E+01	5.57E+00	3.65E−04	6.36E+06	2.85E+10	2.59E−06
0.8	1.95E+01	1.39E+01	4.82E+00	2.13E−04	8.31E+06	5.19E+10	1.65E−06
0.9	2.23E+01	1.65E+01	4.14E+00	1.26E−04	1.10E+07	9.19E+10	1.04E−06
1.0	2.51E+01	1.92E+01	3.53E+00	7.53E−05	1.46E+07	1.59E+11	6.57E−07
1.1	2.79E+01	2.20E+01	2.99E+00	4.57E−05	1.96E+07	2.71E+11	4.13E−07
1.2	3.07E+01	2.48E+01	2.51E+00	2.80E−05	2.64E+07	4.53E+11	2.59E−07
1.3	3.34E+01	2.76E+01	2.09E+00	1.74E−05	3.57E+07	7.48E+11	1.61E−07
1.4	3.61E+01	3.04E+01	1.73E+00	1.09E−05	4.85E+07	1.22E+12	9.93E−08
1.5	3.87E+01	3.32E+01	1.43E+00	6.85E−06	6.62E+07	1.98E+12	6.02E−08
1.6	4.11E+01	3.59E+01	1.17E+00	4.33E−06	9.07E+07	3.20E+12	3.56E−08
1.7	4.33E+01	3.86E+01	9.51E−01	2.73E−06	1.25E+08	5.14E+12	2.04E−08
1.8	4.52E+01	4.11E+01	7.69E−01	1.70E−06	1.73E+08	8.23E+12	1.12E−08
1.9	4.68E+01	4.34E+01	6.19E−01	1.02E−06	2.40E+08	1.32E+13	5.75E−09
2.0	4.80E+01	4.54E+01	4.96E−01	5.82E−07	3.34E+08	2.10E+13	2.75E−09
2.1	4.88E+01	4.70E+01	3.96E−01	3.08E−07	4.68E+08	3.36E+13	1.21E−09
2.2	4.94E+01	4.81E+01	3.16E−01	1.50E−07	6.57E+08	5.37E+13	4.93E−10
2.3	4.97E+01	4.89E+01	2.51E−01	6.74E−08	9.26E+08	8.58E+13	1.87E−10
2.4	4.99E+01	4.93E+01	2.00E−01	2.83E−08	1.31E+09	1.37E+14	6.72E−11
2.5	5.01E+01	4.96E+01	1.59E−01	1.13E−08	1.84E+09	2.18E+14	2.31E−11

self-consistently generates a suitably truncated form of the density profile (16a), and then multiplying this by the volume of phase space associated with energies in the range $(E+dE, E)$ (e.g. Binney 1982b). In Table 1 we give this estimate of $M(E)$ for Schwarzschild's model, together with the mass $M(r)$ interior to radius r. Notice that at large binding energy E, $M(E) \propto (E_{\max}-E)^3$, where $E_{\max}$ is the absolute value (4π) of the central gravitational potential, and that at small binding energies, $M(E) \rightarrow M\{r(E)\}$, where $r(E)$ is the radius at which the absolute value of the potential is E. Table 1 also gives the distribution function $f(E)$ that self-consistently generates a truncated form of (16a), and estimates of the dynamical and dissolution times $\tau_{\rm dyn}$ and $\tau_{\rm dis}$ in Schwarzschild's model when the latter is scaled to $r_c=240$ pc and $\sigma_0=240\,{\rm km\,s^{-1}}$ and contains a central object of mass $m=0.02M_c \simeq 10^8 M_\odot$. From the table, $\tau_{\rm dis} \simeq 10^{10}$ yr for $a \simeq 3.5 r_c$.

In Fig. 9 we plot from equation (31) for five values of μ, the accretion rate $\dot{m}(E)$ in Schwarzschild's model scaled in the standard way. The results of Fig. 9 can be scaled to other values of r_c and σ_0 by shifting the curves by $\log_{10}(r_c/\sigma_0)$ to the right, and by $\log_{10}(\sigma_0^{11/3} r_c^{-2/3}/240^3)$ upwards. Notice that although the initial accretion rate scales as $\mu^{4/3}$, the current rate is a *declining* function of μ when $\mu > 0.02$, because large central objects have already either eaten or scared away all their most accessible prey. The maximum current accretion rate, $\dot{m} \simeq 5\times10^{-6} M_\odot\,{\rm yr^{-1}}$, occurs for $\mu \simeq 0.02$.

It is interesting to compare this accretion rate with the value expected in the case of a spherical galaxy (Frank & Rees 1976; Lightman & Shapiro 1977; Frank 1978). The rate at which a black hole at the centre of a spherical system accretes stars is given by the rate at which two-body encounters scatter stars into the so-called 'loss cone' of low-angular momentum orbits. This process is characterized by the angle

$$\Delta\theta < \sqrt{\left(\frac{10\ln N}{N}\right)} \simeq 2.1\times10^{-4}\left(\frac{\sigma_0}{240\,{\rm km\,s^{-1}}}\right)^{-1}\left(\frac{r_c}{240\,{\rm pc}}\right)^{-1/2}{\rm rad}, \tag{32}$$

where N is the effective number of stars in the core, through which two-body encounters typically deflect the velocity vectors of core stars in one dynamical time. This angle in turn defines the radius

$$r_{\rm crit} = \frac{L_t}{\sigma_0 \Delta\theta} = 85\left(\frac{m}{10^8 M_\odot}\right)^{2/3}\left(\frac{r_c}{240\,{\rm pc}}\right)^{1/2}{\rm pc} \tag{33}$$

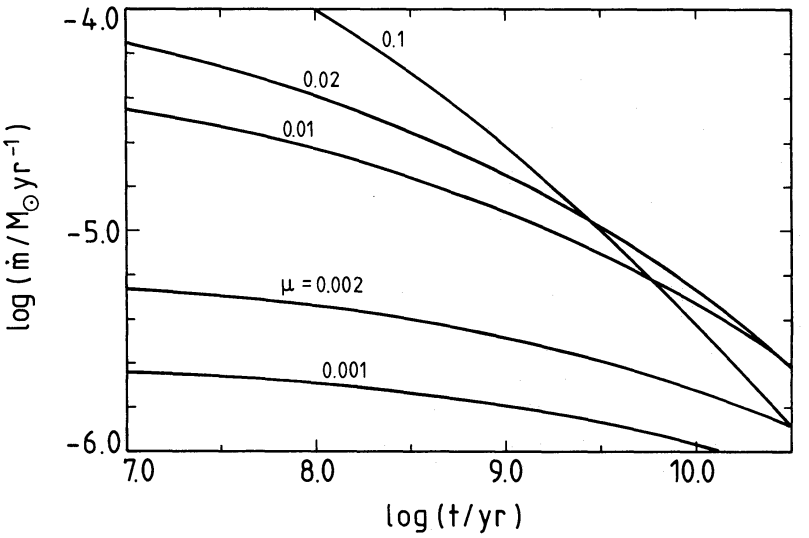

Figure 9. The accretion rate $\dot{m}$ predicted by equation (31) for a black hole with mass μM_c placed at the centre of a standard triaxial galaxy.

beyond which zero-angular momentum orbits begin to be heavily populated. For $r_{\rm crit}$ comparable with r_c, a reasonable estimate of the hole's accretion rate is

$$\dot{m}_{\rm lc} \simeq \frac{M_c (r_{\rm crit}/r_c)^3}{t_R \ln(2/\theta_c)}$$

$$\simeq 1.9\times10^{-1}\left(\frac{m}{10^8\,M_\odot}\right)^2\left(\frac{\sigma_0}{240\,{\rm km\,s^{-1}}}\right)\left(\frac{r_c}{240\,{\rm pc}}\right)^{-5/2} M_\odot\,{\rm yr}^{-1}, \tag{34}$$

where $\theta_c \simeq b_t/r_{\rm crit}$ is the loss-cone angle at $r_{\rm crit}$ and t_R is the standard Spitzer & Härm (1958) relaxation time. Thus at the present epoch the accretion rate of a $10^8\,M_\odot$ black hole at the centre of a triaxial galaxy is at least an order of magnitude larger than that of an identical hole in a similar spherical galaxy.

5 Central density cusps

In the last few years much controversy has been excited by the question of whether stellar densities tend to flatten off close to the centres of giant elliptical galaxies, or whether the density is continuing to rise at the smallest radii ($r \simeq 200$ pc) accessible to ground-based observations. Recent work by Lauer (1985) and Kormendy (1985, in preparation) has tended to confirm the view articulated earlier by Schweizer (1979) that the stellar density in many giant elliptical galaxies is still rising at small radii. In the light of the conclusion of the last section, that a massive central object will in the long run destroy triaxiality, it is clearly important to determine whether triaxiality is compatible with central density cusps of the type observed. Hence in this section we investigate the orbital structures of systems with density distributions of the form

$$\varrho_p(r) = \varrho_0 a^{-p} \tag{35a}$$

where

$$a(r) \equiv \left(x^2 + \frac{y^2+z^2}{q_\varrho^2}\right)^{1/2} \tag{35b}$$

and

$$p \equiv \begin{cases} p & a<10r_c \\ 4 & a\geq 10r_c \end{cases}. \tag{35c}$$

These density distributions form prolate bodies with axis ratio $q_\varrho<1$. The axisymmetry of these systems is entirely a matter of convenience in solving for the required potentials; in the plane $z=0$ in which we compute orbits, the potentials of these axisymmetric bodies do not differ greatly from those of the triaxial bodies that we actually wish to study.

At $a\geq 10r_c$ the density distribution (35) falls off in the manner roughly characteristic of an $r^{1/4}$ model at radii exceeding the effective radius (Young 1976; Jaffe 1983). At $a\leq 10r_c$ the density (35) declines as the $p^{\rm th}$ power of radius; an $r^{1/4}$ model is approximated by setting $p=0.75$ (Young 1976).

In the spherical case $q_\varrho=1$, the mass contained within radius r is

$$M(r) = \frac{4\pi\varrho_0}{3-p} r^{3-p} \qquad (r<10r_c). \tag{36}$$

Hence three ranges of p should be distinguished:

(C1) $p<1$: The radial force $F\propto r^{1-p}$ tends to zero at small r, as in a model with a homogeneous core.

(C2) $1 \leqslant p \leqslant 2$: F diverges at small r, but the circular speed $v_c \propto r^{2-p}$ does not.

(C3) $2 < p$: Both F and v_c diverge at small r as in the case of Keplerian motion about a point mass.

For any value of p we obtain the corresponding gravitational potential as a sum of terms involving Legendre polynomials $P_n(\cos\theta)$, where θ is the angle between the radius vector r and the long axis of the potential. In our orbit calculations, we have included polynomials up to and including P_8.

We wish to compare the orbital structure supported by the potential associated with the density distributions (35) for p in each of the three ranges (C1) to (C3) above with the orbital structures associated with density distributions which remain finite as $r \to 0$. In particular we study:

(H1) Motion in the approximation of de Zeeuw & Merritt (1983) to Schwarzschild's (1979) potential.

(H2) Motion in the logarithmic potential (8) $\Phi_{\rm Sch}$.

(H3) Motion in a Stäckel potential (Landau & Lifshitz 1975; de Zeeuw 1985a, b; Gerhard 1985)

$$\Phi_{\rm StL} = \frac{\lambda \ln(\lambda + r_c^2) - \mu \ln(\mu + r_c^2)}{\lambda - \mu} \tag{37}$$

where λ and μ are confocal ellipsoidal coordinates ($\lambda \geqslant \mu$).

(H4) Motion in the Stäckel potential

$$\Phi_{\rm StS} = \frac{f(\lambda) - f(\mu)}{\lambda - \mu} \tag{38a}$$

with

$$f(\lambda) = \beta^{1/2}\lambda^{1/2}\left[\ln\left\{\frac{(\lambda+\beta)+\lambda^{1/2}(\lambda+2\beta)^{1/2}}{\beta}\right\} + \arcsin\left(\frac{\beta}{\lambda+\beta}\right) - \tfrac{1}{2}\pi\right]$$

$$-2\lambda\left\{1-\left(\frac{\beta}{\lambda}\right)^{1/2}\right\}\arctan\left\{\left(\frac{\lambda}{\beta}\right)^{1/2}\right\}, \tag{38b}$$

$$f(\mu) = |\beta\mu|^{1/2}\left[\ln\left\{\frac{\beta+|\mu|^{1/2}(\mu+2\beta)^{1/2}}{(\beta^{1/2}+|\mu|^{1/2})^2}\right\} + \arcsin\left(\frac{\mu+\beta}{\beta}\right) - \tfrac{1}{2}\pi\right] - 2\mu. \tag{38c}$$

This corresponds to a prolate system with density along the minor axis $\varrho = \varrho_0\{\beta/(z^2+\beta)\}^{3/2}$, and was calculated via Kuzmin's theorem (de Zeeuw 1985b), with $2\pi G\varrho_0\beta = 1$.

For the potentials generated by the density distributions (35) we have set the axis ratio $q_\varrho = 0.625$ for comparison with Schwarzschild's potential. In the logarithmic potential (8) the choice $q = 0.83$ corresponds to a density distribution with $q_\varrho \simeq 0.625$ for $r > 5r_c$, slowly rising to $q_\varrho \simeq 0.75$ near $r = 0$. The Stäckel potential (37) has a radial density profile $\varrho \propto r^{-2}$, and the interfocal length $\sqrt{\beta}$ of the coordinate system has been adjusted to give an axis ratio $q_\varrho \simeq 0.625$ within the core; outside the core the isodensity surfaces rapidly become round $\{q_\varrho(3r_c) \simeq 0.75;\ q_\varrho(10r_c) \simeq 0.98\}$. Finally, the potential (38) corresponds to $\varrho \propto r^{-3}$, with $q_\varrho = 0.78$ in the core, $q_\varrho(3r_c) \simeq 0.84$, and $q_\varrho(10r_c) \simeq 0.91$.

5.1 LOOP-ORBIT FRACTION

For each of the potentials (C1)–(H4) we study the structure of orbits confined to the plane $z = 0$. Many such orbits are loop orbits; i.e. orbits on which stars have a definite sense of circulation about the centre and avoid a neighbourhood of the origin. These orbits all generate density distributions aligned perpendicular to the bar. Hence a self-consistent system will be exceedingly

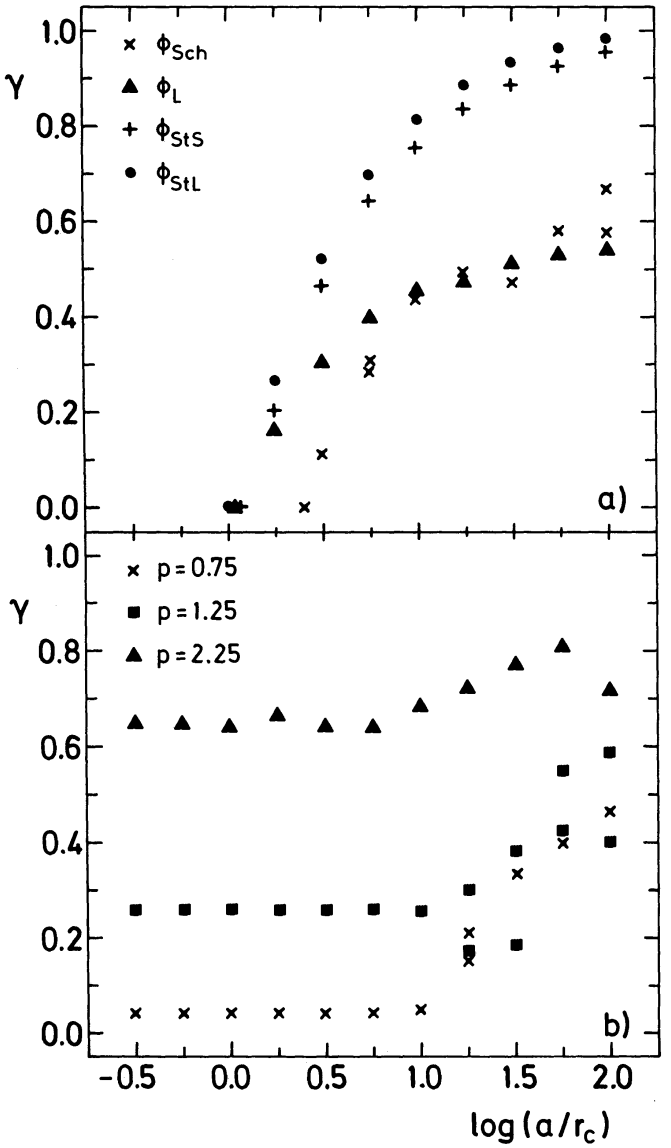

Figure 10. The loop orbit fraction γ defined by equation (39) as a function of apocentric radius a in the potentials of (a) four models with homogeneous cores, and (b) three two-power-law density distributions defined by equations (35). When a curve has upper and lower branches, the upper branch includes resonant loop orbits and associated stochastic orbits.

hard to construct if most of phase space is occupied by the loop orbits: if $d\tau_t$ is the volume of phase space available to all orbits with energies in some small range, and $d\tau_l$ is the volume of phase space occupied by the loop orbits with energies in the same range, then a self-consistent bar is probably feasible only if the quantity

$$\gamma(E) = \frac{d\tau_l}{d\tau_t} \tag{39}$$

is significantly less than unity over a wide range of energies E.

The total phase-space volume $d\tau_t$ may be obtained from the integral

$$\frac{d\tau_t}{dE} = 2\pi \int dx\, dy \tag{40}$$

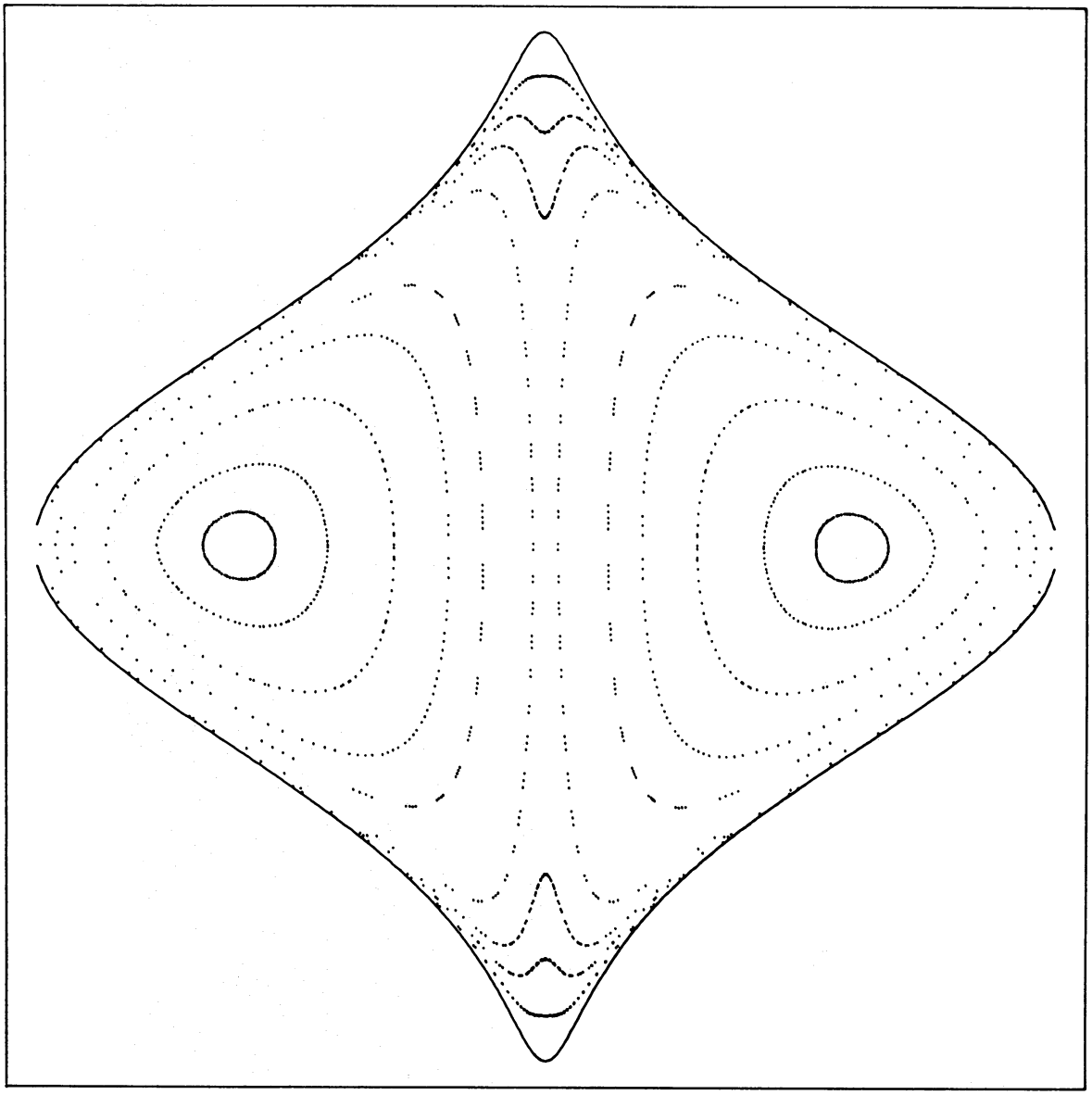

(a)

Figure 11. $(x, \dot{x})$ surface of section for motion at the energy corresponding to apocentre distance $a=15r_c$ in (a) the Stäckel potential (37), and (b) Schwarzschild's potential.

where the integration is over all values of the coordinates for which $v^2 \equiv 2(E-\Phi)>0$. The corresponding volume $d\tau_l$ occupied by the loop orbits is harder to evaluate. If we denote the radial action of a loop orbit by J_r and its angular frequency by ω_ϕ, we have (Binney *et al.* 1985)

$$\frac{d\tau_l}{dE} = 2(2\pi)^2 \int_0^{J_r(\max)} \frac{dJ_r}{\omega_\phi} \tag{41}$$

where $J_r(\max)$ is the radial action of the most eccentric loop orbit and the first factor 2 accounts for the two possible senses of circulation of loop orbits. We have obtained the actions J_r and frequencies ω_ϕ of loop orbits in the potentials studied by the spectral technique of Binney & Spergel (1984). Analytic expressions are available (e.g. Gerhard 1985) for the actions and frequencies of orbits in the Stäckel potentials (37) and (38). We find that the values of J_r and ω_ϕ obtained by spectral analysis of orbits in the potential (37) agree to within 2 per cent with the analytic values.

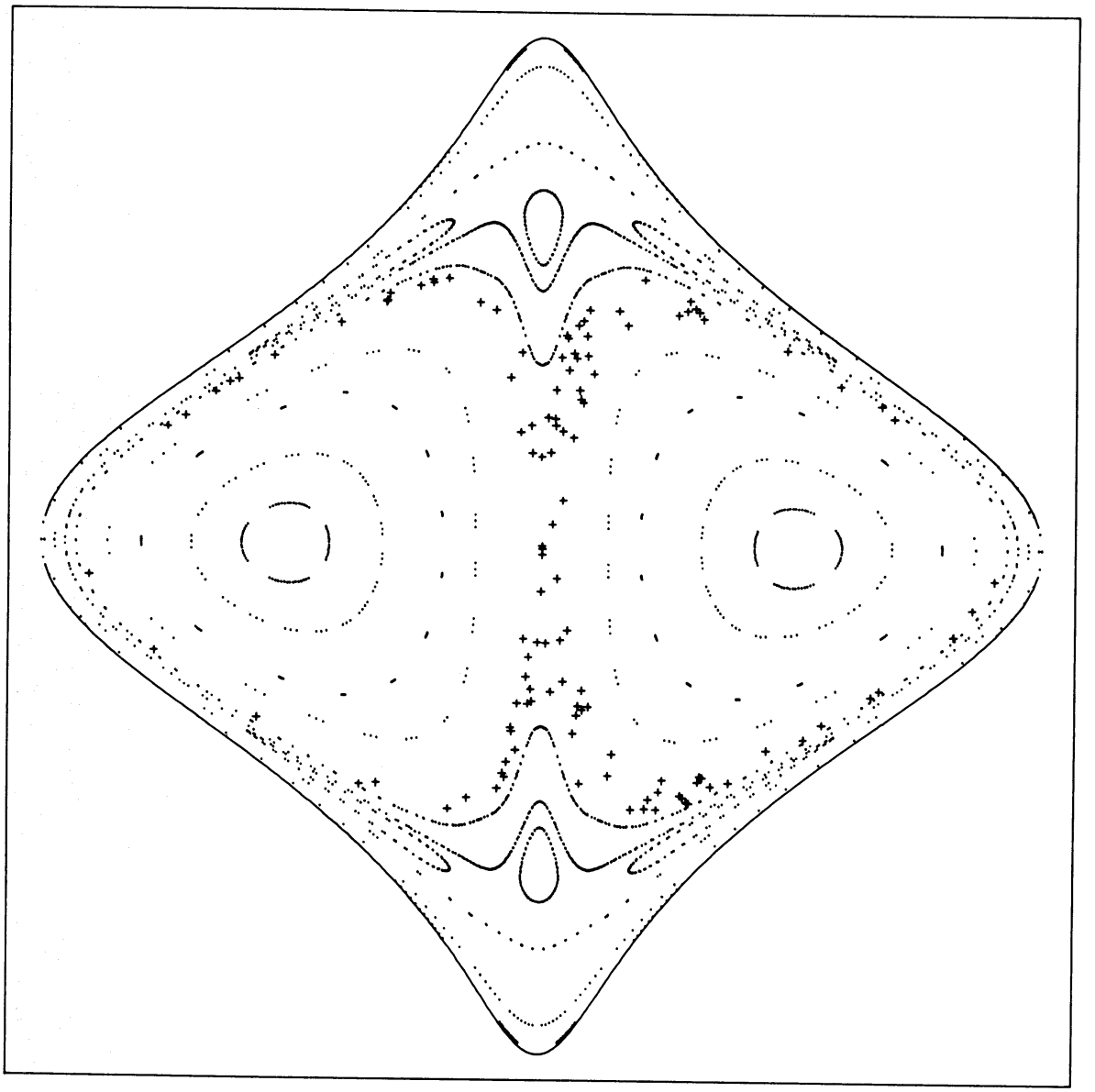

(b)

Figure 11 – *continued*

Fig. 10 shows plots for each of the potentials studied here of the loop orbit fraction γ versus the furthest distance a that the orbit's energy allows it to go down the long axis of the potential. The plotted values of γ are accurate to $\simeq 3$ per cent except for the inner parts of the $p=2.25$ curve in Fig. 10b, which may be rather more than 5 per cent in error. In some potentials, the curve $\gamma(a)$ is split through a range of a; in these cases the upper branch shows the result of including the phase-space volume of a band of resonant and semi-stochastic loop orbits, while the lower branch shows the loop fraction less these orbits.

Fig. 10a shows γ for the four models with homogeneous cores. In each case the loop-orbit fraction is zero for very small a because in an harmonic potential all orbits are box orbits. γ increases rapidly as a increases through $a \simeq 2r_c$ and the star begins to perceive a more nearly central potential. In the logarithmic potential (8), $\gamma \rightarrow 55$ per cent at large a, while in Schwarzschild's potential, $\gamma \simeq 60$ per cent and is still rising at $100r_c$. In the Stäckel potentials (37) and (38), $\gamma \simeq 1$ at $100r_c$ essentially independently of the slope of the density profile, or of the

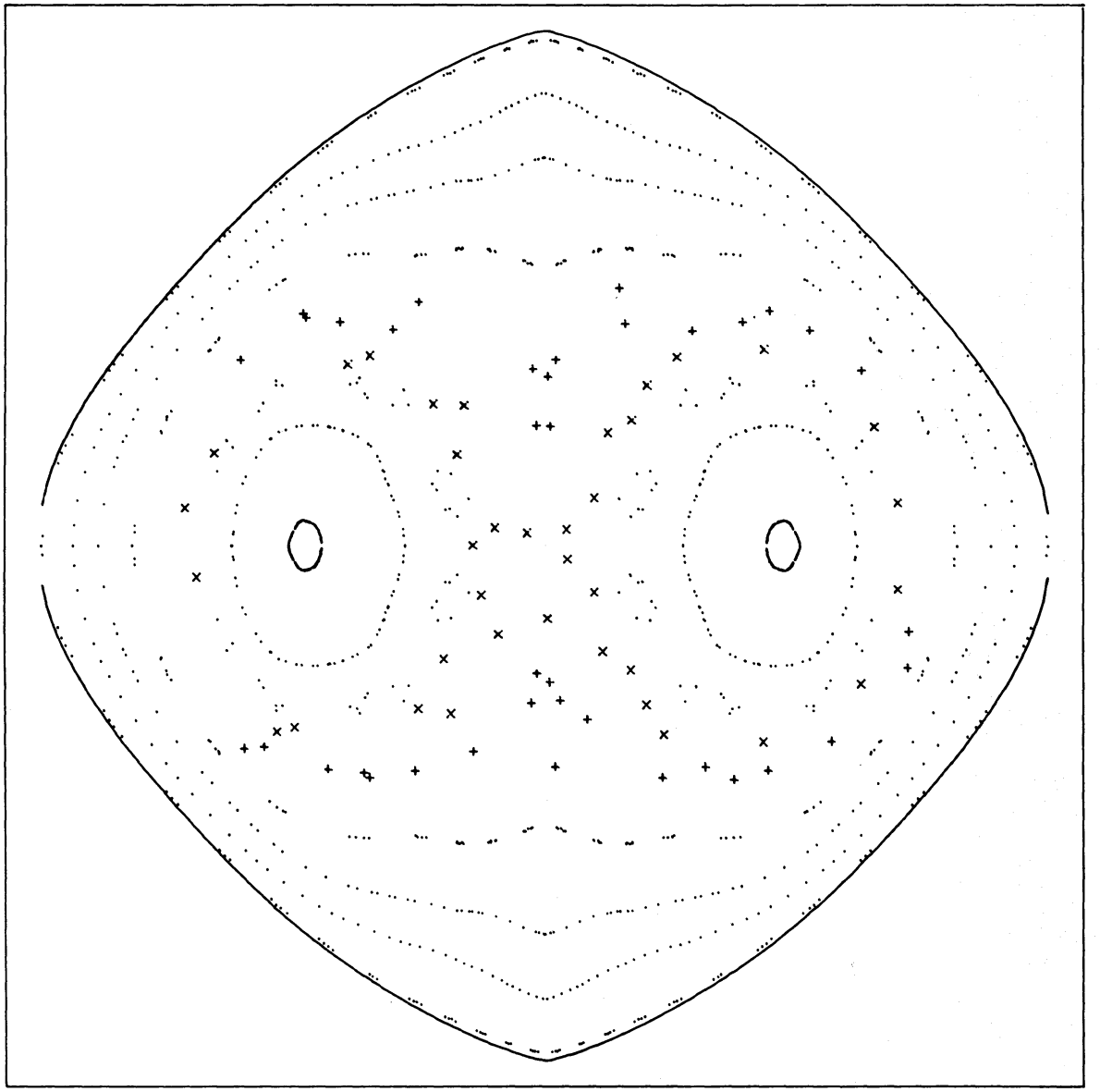

(a)

Figure 12. $(x, \dot{x})$ surface of section in the potential of the two-power approximation (35) to an $r^{1/4}$ model for apocentric distance (a) $a=18r_c$, and (b) $a=1.8r_c$.

central axis ratio of the underlying density distribution; only the detailed shape of the curve $\gamma(a)$ between $\gamma(r_c)\simeq 0$ and $\gamma(100r_c)\simeq 1$ depends on the form of the potential.

Fig. 10b shows the corresponding results for potentials generated by the density distributions (35) for three values of p. The choice $p=0.75$ which yields the best two-power-law approximation to an $r^{1/4}$ model, gives a loop fraction γ which is very small ($\simeq 4$ per cent) for $a<10r_c$, and rises to $\gamma\simeq 45$ per cent at large a. Thus a large portion of phase space is available to box orbits in this potential. When we set $p=1.25$, which corresponds to a singular central force but a non-divergent central circular speed, we still find that less than half of phase space is occupied by loop orbits at low energies, although $\gamma(a<10r_c)\simeq 26$ per cent is more than 5 times larger than the corresponding number for the case $p=0.75$. When $p=2.25$ a large proportion of phase space is occupied by loop orbits at all energies.

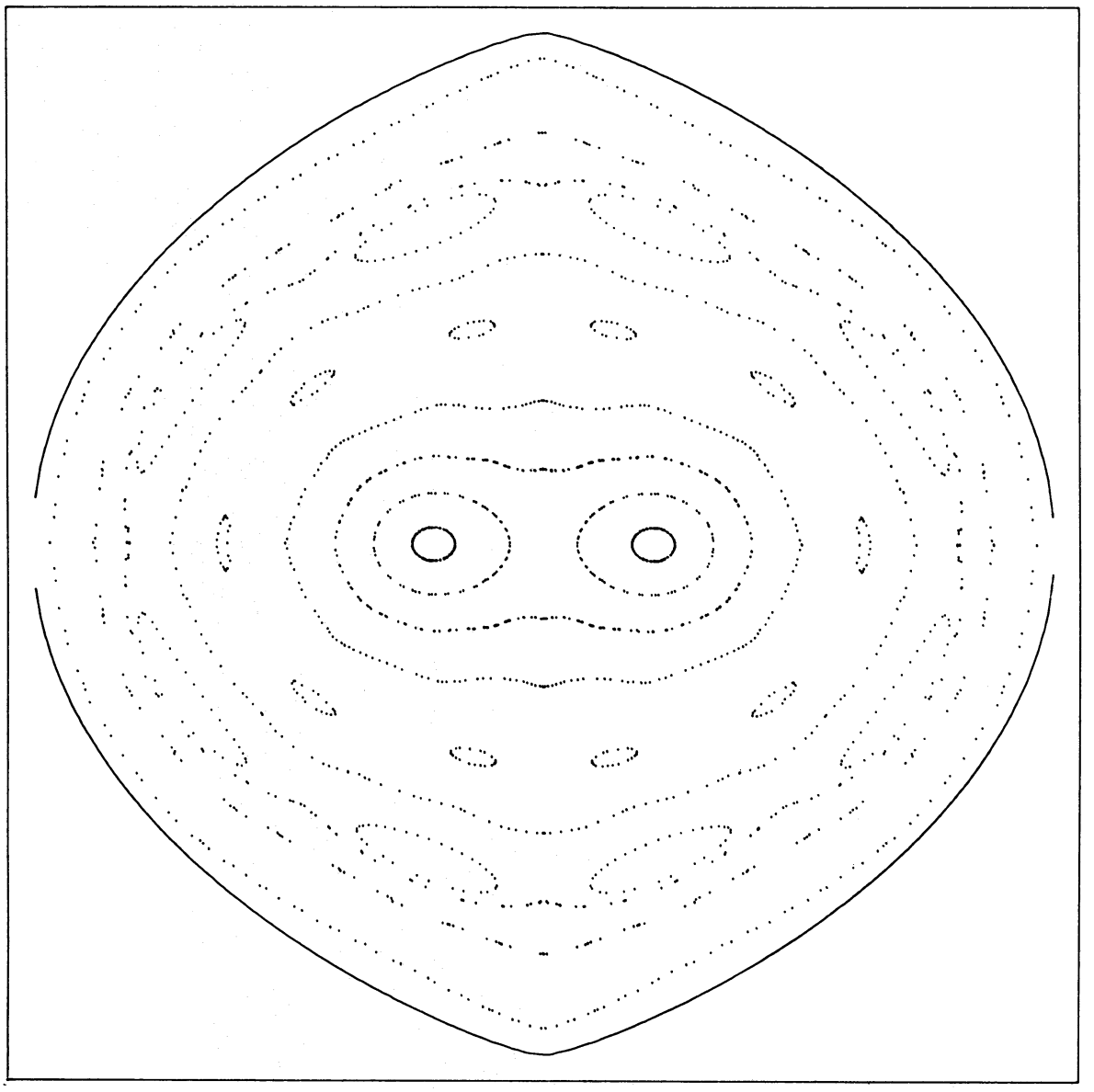

(b)

Figure 12 – *continued*

5.2 NON-LOOP ORBITS

Since loop orbits in a non-rotating potential all have density distributions that tend to oppose the bar, these orbits cannot be heavily populated in any self-consistent stellar bar. Hence we next examine the non-loop orbits.

In the Stäckel potentials (37) and (38), all the non-loop orbits are regular box orbits (Fig. 11a). In Schwarzschild's potential and the logarithmic potential (8) most, but not all, non-loop orbits are boxes: In addition to the standard box orbits these potentials support a few small families of resonant box orbits and some stochastic orbits. The resonant families generate the chains of islands visible in Fig. 11b, which is a surface of section of motion in Schwarzschild's potential.

Fig. 12a is a surface of section for motion at a comparable energy in the $r^{1/4}$-like potential obtained from (35) when $p=0.75$. The general appearance of this diagram is very similar to that of Fig. 11b except for the chain of islands surrounding the loops, and a large stochastic layer. At the

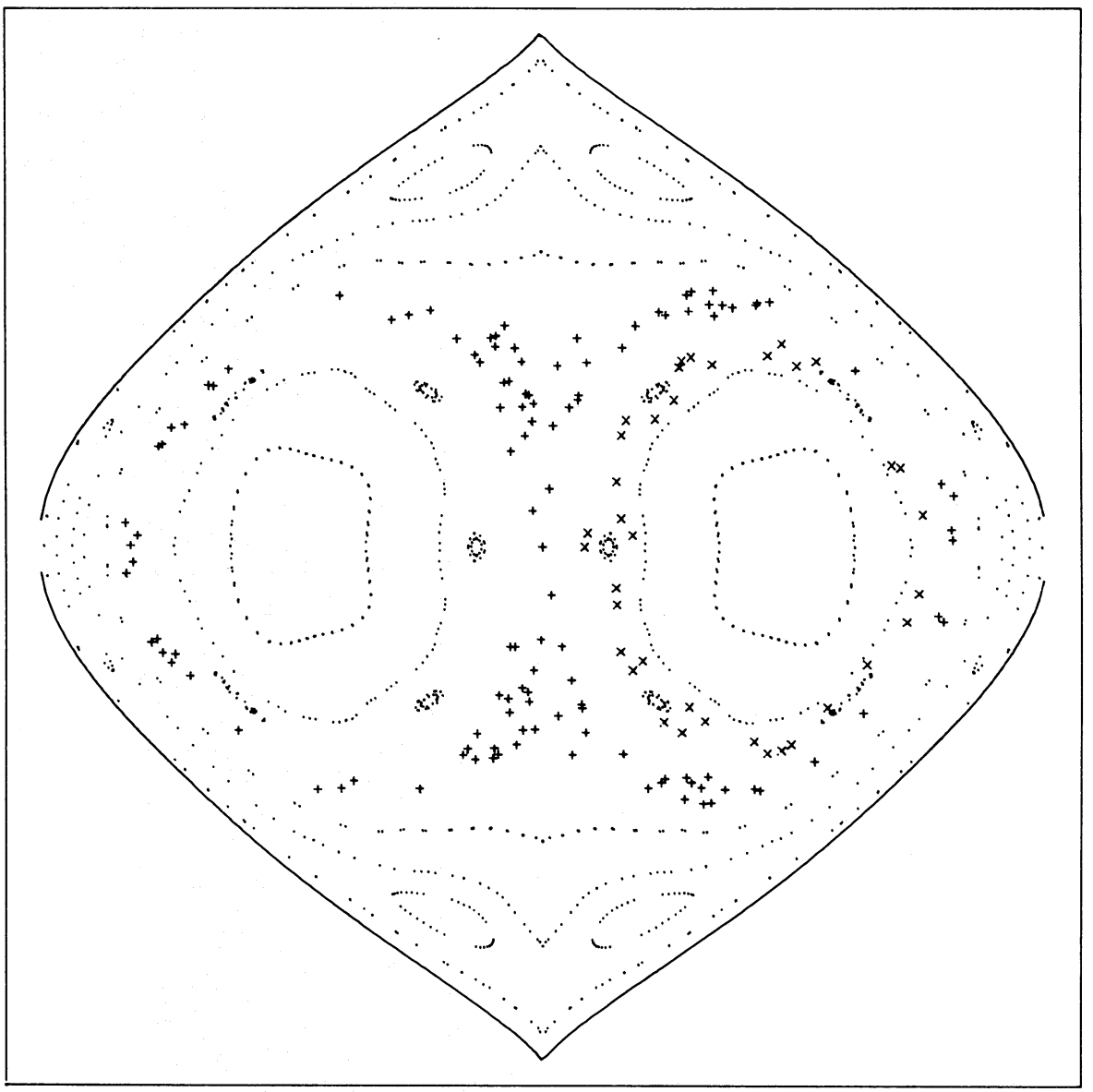

Figure 13. $(x, \dot{x})$ surface of section for motion with $a=18r_c$ in the potential of the model obtained by setting $p=1.25$ in equation (35). This system generates a singular central force.

energy of Fig. 12a, near that associated with the power-law break in (35) at $r=10r_c$, the irregularity of the orbits is maximal. Surfaces of section at lower energies look much more regular (Fig. 12b); notice that in the range $2<a/r_c<10$, box orbits are significantly more prominent in the $r^{1/4}$-like potential than in Schwarzschild's potential. These box orbits have waists of non-zero width.

From Fig. 12 we conclude that the planar orbit structure of potentials generated by bodies with $r^{1/4}$-like central density cusps is characterized by the same box- and loop-orbit families that are supported by Schwarzschild's potential. In particular, thin box orbits with waists of finite width exist at all energies, so there seems every reason to believe that self-consistent triaxial models can be constructed that have the radial density profile of the $r^{1/4}$ model.

Fig. 13 shows a surface of section equivalent to Fig. 12a for the case $p=1.25$, in which the central force diverges as the centre is approached. Loop and box orbits may again be distinguished. However, the largest families of resonant box orbits occupy more of the surface of

section associated with the more centrally concentrated potential with $p=1.25$ than in the case $p=0.75$. The stochastic layer between the loops and the boxes is even somewhat thinner when $p=1.25$. Increasing p to 2.25 substantially eliminates the box orbits; most orbits now appear to belong to resonant families whose members avoid the origin.

It is natural to enquire whether even in the absence of a black hole, the harmonic core of a potential with such a core can generate stochasticity by acting as a scattering centre for orbits of sufficiently high energy. We know analytically that in Stäckel potentials such as (37) and (38), all orbits are strictly regular. Fig. 14 shows surfaces of section for motion at high energies in the logarithmic potential (8) and in Schwarzschild's potential. Fig. 14a shows that orbits in the logarithmic potential remain regular at high energies, while high-energy non-loop orbits in Schwarzschild's potential tend to be irregular (Fig. 14b). From Fig. 14a one sees that the explanation for this very different behaviour is that at high energies many non-loop orbits in the logarithmic potential tend to be trapped by 4:3, 3:2 and 1:2 resonances. Such orbits avoid the very centre of the potential, and thus avoid being scattered. In Schwarzschild's potential these resonances compete less successfully with numerous other resonances, or interact more strongly between themselves (Chirikov 1979). Irregularity may then be thought of as arising either because orbits are scattered by the core, or as a consequence of competition between different resonances.

6 Conclusions

In time, the box orbits that form the backbone of a triaxial elliptical galaxy carry stars arbitrarily close to the centre. Analytic (de Zeeuw 1985a) and numerical (Aarseth & Binney 1978; Schwarzschild 1979) models of triaxial ellipticals assume that these systems have homogeneous cores in which the gravitational potential is approximately quadratic in the coordinates, and it has often been suggested (e.g. de Zeeuw & Merritt 1983) that box orbits are a natural consequence of this form of potential. In this paper we have investigated the consequences for box orbits and triaxiality of placing a compact object or a density cusp at the galactic centre, thus eliminating the region in which the potential is a quadratic function of the coordinates.

Analytic estimates and numerical orbit integrations have been used to study the effect of a central massive body with $\simeq 2$ per cent of the mass of the core on the orbital structure of the underlying galaxy. We find that such a massive central object turns over to the loop orbits much of phase space at energies such that stars are confined to the core. If the central object is soft, box orbits persist outside the radius within which the object dominates the gravitational field, but as the object is hardened, resonances and associated stochastic layers begin to break up the region of phase space formerly occupied by regular boxes. For a softening radius smaller than about twice the impact parameter for large-angle deflection by the central body, this region forms a single stochastic sea.

While any point mass at the galactic centre makes all non-resonant box orbits strictly speaking irregular, these orbits often closely resemble regular box orbits for many dynamical times. In particular, in the presence of a point mass, a single stellar trajectory can be represented by a sequence of segments of regular box orbits, joined by relatively close encounters of the star with the central body. We find that the probability that a stellar trajectory shifts from one regular box segment to another on a given passage by the centre is approximately equal to the probability that the star encounters the nucleus at an impact parameter smaller than three times the impact parameter for a 90° deflection. Thus the total cross-section for such scattering encounters is much larger than the cross-section for hard encounters.

The rate at which a star experiences scattering encounters with a central object is a rapidly decreasing function of increasing apocentric radius a. There are three contributions to this

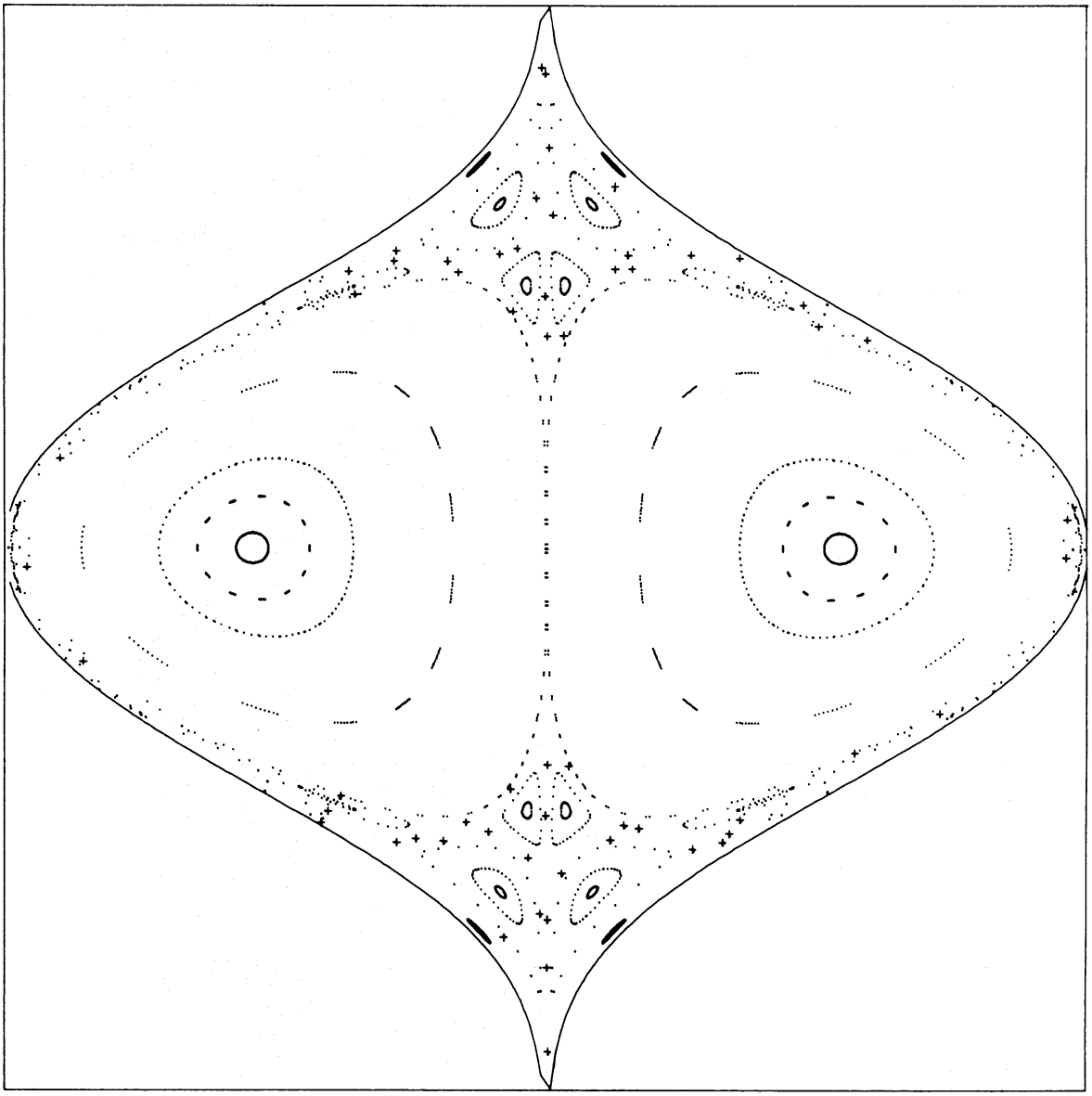

(a)

Figure 14. $(x, \dot{x})$ surfaces of section for motion at high energies ($a=100r_c$) in potentials with harmonic cores. (a) The logarithmic potential (8), and (b) Schwarzschild's potential. At these energies regular non-resonant box orbits have been replaced by 3:2, 4:3 and 2:1 resonant orbits, and irregular orbits. The logarithmic potential supports many regular resonant orbits, while most orbits in Schwarzschild's potential are highly irregular. In each case the crosses are generated by a single stochastic orbit.

decrease: (i) The dynamical time increases with a. (ii) The area of the waist of a typical box orbit increases with a. (iii) The impact parameter for a hard encounter decreases with a. In a typical giant elliptical galaxy, most stars on box orbits with apocentric radii $a \leqslant 1$ kpc would by now have suffered at least one scattering encounter with a central object containing $\simeq 2$ per cent of the galaxy's core mass, while the majority of stars on larger box orbits would still be on their first regular orbital segment. The *smaller* the galaxy's core radius, the *larger* is the radius $a_{\rm dis}$ out to which a central object of given mass will have scattered most box orbits; $a_{\rm dis} \propto r_c^{-1/2}\sigma_0^{13/2}$ for fixed m and $a_{\rm dis} > 5r_c$.

Unless the gravitational potentials of elliptical galaxies rotate much more rapidly than is

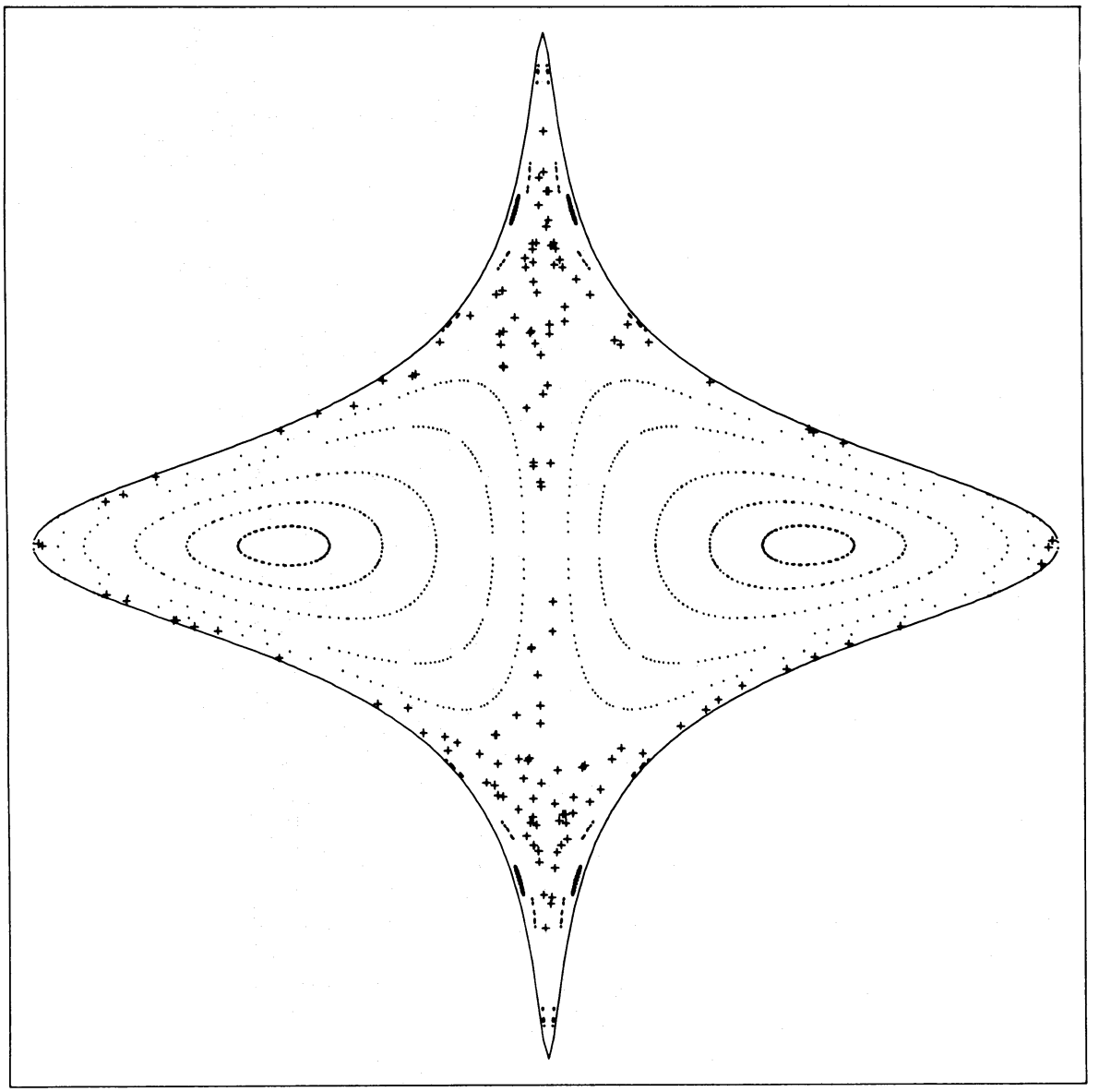

(b)

Figure 14 – *continued*

currently thought possible (e.g. Binney 1982a; Schwarzschild 1982), these results for non-rotating potentials will be unaffected by realistic rates of figure rotation.

Repeated scattering of stars from one box orbit to another will tend to establish a uniform distribution of stars within the region of phase space that is accessible to box orbits of given energy. Such a distribution is almost certainly incapable of self-consistently sustaining a triaxial figure. Hence a central black hole must in the long run destroy a non-rotating bar. A simple estimate of the degree to which triaxiality of the potential at radius a depends on the triaxility of the density at the same radius, suggests that scattering of stars by a central object will gradually eliminate a self-consistent bar, from the inside outwards. In a typical elliptical galaxy, a central object with 2 per cent of the core mass would have markedly reduced triaxiality interior to $a \simeq 1$ kpc by the present epoch. In nearby galaxies this effect may be detectable from the ground. In this connection it is interesting that Hummel, Kotanyi & Ekers (1983) and Disney, Sparks & Wall (1984) have claimed that radio-loud ellipticals, which are probably powered by massive

black holes in their nuclei (Lynden-Bell 1969; Rees 1984), are systematically rounder than similar radio-quiet ellipticals (but see also Dressel 1981). However, very massive central objects ($m>10^9\,M_\odot$) and very small core radii ($r_c<10$ pc) must be postulated if this effect, which pertains to the ellipticity at R_{25}, is to be interpreted as due to the destruction of triaxiality by a central black hole.

The calculations on which these results are based have been restricted in two important respects; (i) we have only considered two-dimensional orbits, and (ii) we have only calculated orbits in fixed potentials. Norman, May & van Albada (1985) report fully three-dimensional calculations in fixed and self-consistent potentials. Their conclusions are broadly similar to ours, although they consider only very massive central objects ($0.08\leqslant\mu\leqslant0.4$), and in all their self-consistent field calculations the central object is extremely soft ($\varepsilon=0.27r_c$). Our study complements their work by using surfaces of section to show how any central point mass destroys the regular box orbits that form the backbone of a triaxial elliptical, and to develop a quantitative description of the diffusion of stars through phase space to which scattering of stars by a central mass gives rise. Our analysis enables us to estimate the rates at which a central object (i) destroys triaxiality, and (ii) tidally disrupts stars. The rates at which the models of Norman, May & van Albada (1985) grow round are only partly determined by their central objects, being in part determined by deficiencies inherent in currently available n-body programs, but their rates are broadly in agreement with our results.

As Norman & Silk (1983) and Duncan & Shapiro (1983) have remarked, a triaxial potential is capable of feeding stars on to a central black hole more rapidly than two-body encounters in an axisymmetric potential. We have used the scattering picture developed in Section 3 to estimate the rate $\dot{m}(t)$ at which a $10^8\,M_\odot$ black hole at the centre of a typical triaxial elliptical disrupts stars. We find this rate to be a rapidly decreasing function of time, but the current rate for a $10^8\,M_\odot$ hole, $\dot{m}\simeq5\times10^{-6}\,M_\odot\,\mathrm{yr}^{-1}$, is still more than an order of magnitude greater than the rate at which an identical hole in an axisymmetric galaxy would disrupt stars. The accretion rate of a hole at the centre of a triaxial system is clearly inadequate as an energy source for a luminous quasar. If Seyfert galaxies and radio galaxies can be powered by accretion on to spinning holes at rates as low as $10^{-3}\,M_\odot\,\mathrm{yr}^{-1}$ (Rees 1984), it is just conceivable that these objects feed by disrupting stars on box orbits. However, accretion rates as large as $10^{-3}\,M_\odot\,\mathrm{yr}^{-1}$ can be achieved only very briefly, and for abnormally small core radii r_c. Furthermore, the current rate is a *decreasing* function of increasing black hole mass. Thus the conclusion seems inescapable that these systems are fuelled by loose gas, rather than stars. However, triaxiality of the central gravitational potential may nevertheless play a role, by enhancing the rate at which gas spirals towards the nucleus.

N-body simulations (van Albada 1983; McGlynn 1984; Villumsen 1984) suggest that violent relaxation from cold, irregular initial conditions leads to stellar systems more akin to the $r^{1/4}$ model than a lowered isothermal, and there is some observational evidence that many giant ellipticals do indeed have central density cusps (Schweizer 1979; Lauer 1985). In Section 5 we showed that contrary to what one might expect by a naïve extrapolation of our results for compact central objects, such systems do support box orbits at all energies. Indeed, a two-power-law approximation to the $r^{1/4}$ model supports more regular box orbits at all energies than Schwarzschild's potential. A central density cusp eliminates regular box orbits only if it gives rise to a circular speed which diverges as the centre is approached. Thus there is every reason to believe that triaxial systems can be constructed that have realistic central density cusps.

Acknowledgments

We should like to thank an anonymous referee for a meticulous reading of our manuscript. Part of this work was carried out during at a workshop held at the Weizmann Institute in 1984 July; it is a

pleasure to thank Dr M. Milgrom and his colleagues at the Weizmann Institute for their hospitality during this period.

References

Aarseth, S. J. & Binney, J., 1978. *Mon. Not. R. astr. Soc.*, **185,** 227.
Begelman, M. C., Blandford, R. D. & Rees, M. J., 1984. *Rev. Mod. Phys.*, **56,** 255.
Binney, J. J., 1982a. *Ann. Rev. Astr. Astrophys.*, **20,** 399.
Binney, J. J., 1982b. *Mon. Not. R. astr. Soc.*, **200,** 951.
Binney, J. J., 1982c. *Mon. Not. R. astr. Soc.*, **201,** 15.
Binney, J. J., 1985. *Mon. Not. R. astr. Soc.*, **212,** 767.
Binney, J. J., Gerhard, O. E. & Hut, P., 1985. *Mon. Not. R. astr. Soc.*, **215,** 59.
Binney, J. J. & Petrou, M., 1985. *Mon. Not. R. astr. Soc.*, **214,** 449.
Binney, J. J. & Spergel, D., 1984. *Mon. Not. R. astr. Soc.*, **206,** 159.
Carnahan, B., Luther, H. A. & Wilkes, J. O., 1969. *Applied Numerical Methods*, Wiley, New York.
Chirikov, B. V., 1979. *Phys. Rep.*, **52,** 263.
Contopoulos, G. & Papayannopoulos, T., 1980. *Astr. Astrophys.*, **92,** 33.
de Zeeuw, T., 1985a. *Mon. Not. R. astr. Soc.*, **215,** 729.
de Zeeuw, T., 1985b. *Mon. Not. R. astr. Soc.*, **216,** 273.
de Zeeuw, T. & Merritt, D., 1983. *Astr. J.*, **267,** 571.
Disney, M. J., Sparks, W. B. & Wall, J. V., 1984. *Mon. Not. R. astr. Soc.*, **206,** 899.
Di Tullio, G. A., 1979. *Astr. Astrophys. Suppl.*, **37,** 591.
Dressel, L. L., 1981. *Astrophys. J.*, **245,** 25.
Duncan, M. J. & Shapiro, S. L., 1983. *Astrophys. J.*, **268,** 565.
Eddington, A., 1916. *Mon. Not. R. astr. Soc.*, **76,** 572.
Evans, D. S., 1952. *Mon. Not. R. astr. Soc.*, **112,** 606.
Frank, J., 1978. *Mon. Not. R. astr. Soc.*, **184,** 87.
Frank, J. & Rees, M. J., 1976. *Mon. Not. R. astr. Soc.*, **176,** 633.
Gerhard, O. E., 1983. *Mon. Not. R. astr. Soc.*, **202,** 1165.
Gerhard, O. E., 1985. *Astr. Astrophys.*, in press.
Hohl, F. & Zang, T. A., 1979. *Astr. J.*, **84,** 585.
Hummel, E., Kotanyi, C. G. & Ekers, R. D., 1983. *Astr. Astrophys.*, **127,** 205.
Illingworth, G., 1977. *Astrophys. J. Lett.*, **218,** L43.
Jaffe, W., 1983. *Mon. Not. R. astr. Soc.*, **202,** 995.
King, I. R., 1962. *Astr. J.*, **67,** 274.
King, I. R., 1978. *Astrophys. J.*, **222,** 1.
Kormendy, J., 1982. In: *Morphology & Dynamics of Galaxies*, p. 115, eds Martinet, L. & Mayor, M., Geneva Observatory.
Lake, G. & Norman, C. A., 1983. *Astrophys. J.*, **270,** 51.
Landau, L. D. & Lifshitz, E. M., 1975. *Mechanics*, Pergamon.
Lauer, T. R., 1985. *Astrophys. J.*, **292,** 104.
Lightman, A. P. & Shapiro, S. L., 1977. *Astrophys. J.*, **211,** 244.
Lynden-Bell, D., 1969. *Nature,* **223,** 690.
McGlynn, T. A., 1984. *Astrophys. J.*, **281,** 13.
Norman, C. A., May, A. & van Albada, T. S., 1985. *Astrophys. J.*, in press.
Norman, C. A. & Silk, J., 1983. *Astrophys. J.*, **266,** 502.
Rees, M. J., 1984. *Ann. Rev. Astr., Astrophys.*, **22,** 471.
Sargent, W. L. W., Schechter, P. L., Boksenberg, A., Shortridge, K., Lynds, C. R. & Hartwick, F. D. A., 1978. *Astrophys. J.*, **221,** 731.
Schwarzschild, M., 1979. *Astrophys. J.*, **232,** 236.
Schwarzschild, M., 1982. *Astrophys. J.*, **263,** 599.
Schweizer, F., 1979. *Astrophys. J.*, **233,** 23.
Spitzer, L. & Härm, R., 1958. *Astrophys. J.*, **127,** 544.
van Albada, T. S., 1983. *Mon. Not. R. astr. Soc.*, **201,** 939.
Villumsen, J. V., 1984. *Astrophys. J.*, **284,** 75.
Wilkinson, A. & James, R. A., 1981. *Mon. Not. R. astr. Soc.*, **199,** 171.
Young, P. J., 1976. *Astr. J.*, **81,** 807.
Young, P. J., 1978. *Astrophys. J.*, **217,** 287.
Young, P. J., 1980. *Astrophys. J.*, **242,** 1232.

Appendix: Integration methods and tests

The numerical integrations described in this paper have employed a fourth-order Runge–Kutta algorithm combined with Richardson's extrapolation method (e.g. Carnahan, Luther & Wilkes 1969) for the determination of the time-step length. In this method, the set of first-order differential equations for the phase-space variables x_i is first integrated for two time steps of length Δt. The equations are then integrated from the same initial conditions for a single time step of length $2\Delta t$. The difference between the results of these two integrations yields estimates Δx_i of the truncation errors in the coordinates obtained with two steps of length Δt:

$$\Delta x_i = \frac{1}{15}|x_i(t+\Delta t+\Delta t)-x_i(t+2\Delta t)| \tag{A1}$$

assuming $\Delta x_i \propto (\Delta t)^5$. Any pair of integration steps is rejected, and the integration repeated with smaller time steps, if one of the Δx_i exceeds a specified tolerance δ. The size of the new time steps is determined from the current Δx_i through

$$\Delta t' = \left\{\min\left(\frac{\delta}{\Delta x_i}\right)\right\}^{1/5} \Delta t. \tag{A2}$$

This procedure requires six force evaluations per step. In problems in which the time steps change rapidly and by large factors, the extra expense involved in Richardson's method over a simpler algorithm for choosing step lengths is often marginal, since effort is expended exactly where it is most necessary.

The relation between the cumulative integration error for an orbit and the specified tolerance δ, depends on the stability of the orbit integrated. We have investigated this relation by integrating eccentric elliptic orbits in a Kepler potential. We set $\delta = 10^{10}$, and checked energy, angular momentum, phase and time lag against analytic solutions. After 80 orbital periods, the relative errors in energy for orbits with principal axes b and a were $[\log(\Delta E/E), b/a] = [-7.1, 0.7]; [-6.6, 0.4]; [-6.2, 0.2]; [-5.6, 0.07]; [-5.1, 0.02]$. Angular momentum is typically better conserved than energy. Phase and time lags were checked by evaluating the errors Δt and Δr in the time and radial coordinates when the particle returned to its initial angular position θ_0; we find $0.01\Delta r/r \simeq \Delta t/t \simeq \Delta E/E$ at the end of the calculation. Thus for the calculations reported here $\Delta E/E$ is a good indicator of accuracy. For the integrations reported in Section 3 we have typically accepted a cumulative error $\Delta E/E \leqslant 10^{-5}$.